



# Energy decomposition analysis

Lili Zhao,<sup>1</sup> Moritz von Hopffgarten,<sup>2</sup> Diego M. Andrada<sup>2</sup>  
and Gernot Frenking<sup>1,2,3\*</sup>

The energy decomposition analysis (EDA) is a powerful method for a quantitative interpretation of chemical bonds in terms of three major components. The instantaneous interaction energy  $\Delta E_{\text{int}}$  between two fragments A and B in a molecule A–B is partitioned in three terms, namely (1) the quasiclassical electrostatic interaction  $\Delta E_{\text{elstat}}$  between the fragments; (2) the repulsive exchange (Pauli) interaction  $\Delta E_{\text{Pauli}}$  between electrons of the two fragments having the same spin, and (3) the orbital (covalent) interaction  $\Delta E_{\text{orb}}$  which comes from the orbital relaxation and the orbital mixing between the fragments. The latter term can be decomposed into contributions of orbitals with different symmetry which makes it possible to distinguish between  $\sigma$ ,  $\pi$ , and  $\delta$  bonding. After a short introduction into the theoretical background of the EDA we present illustrative examples of main group and transition metal chemistry. The results show that the EDA terms can be interpreted in chemically meaningful way thus providing a bridge between quantum chemical calculations and heuristic bonding models of traditional chemistry. The extension to the EDA–Natural Orbitals for Chemical Valence (NOCV) method makes it possible to breakdown the orbital term  $\Delta E_{\text{orb}}$  into pairwise orbital contributions of the interacting fragments. The method provides a bridge between MO correlations diagrams and pairwise orbital interactions, which have been shown in the past to correlate with the structures and reactivities of molecules. There is a link between frontier orbital theory and orbital symmetry rules and the quantitative charge- and energy partitioning scheme that is provided by the EDA–NOCV terms. The strength of the pairwise orbital interactions can quantitatively be estimated and the associated change in the electronic structure can be visualized by plotting the deformation densities. © 2017 Wiley Periodicals, Inc.

How to cite this article:  
WIREs Comput Mol Sci 2018, 8:e1345. doi: 10.1002/wcms.1345

## INTRODUCTION

The fundamental physical laws describing the interactions of atoms in molecules exist since the development of quantum mechanics in the beginning

This paper is dedicated to Professor Helmut Schwarz on the occasion of his 75th birthday.

\*Correspondence to: frenking@chemie.uni-marburg.de

<sup>1</sup>Institute of Advanced Synthesis, School of Chemistry and Molecular Engineering, Jiangsu National Synergetic Innovation Center for Advanced Materials, Nanjing Tech University, Nanjing, China

<sup>2</sup>Fachbereich Chemie, Philipps-Universität Marburg, Marburg, Germany

<sup>3</sup>Donostia International Physics Center (DIPC), Donostia, Spain

Conflict of interest: The authors have declared no conflicts of interest for this article.

of the 20th century and its first application on a molecular system in 1927 by Heitler and London.<sup>1</sup> Nevertheless, in chemical science bonding properties are commonly discussed in terms heuristic bonding models that usually do not ground on these fundamental laws but rather on experimental observations which were casted in *ad hoc* concepts. In the 19th century, chemistry widely developed as an experimental science that proved to be essential for the technical and industrial progress. As at that time physics could not give a description of the nature of the strong interactions that keep atoms bound to each other, heuristic models and rules were deduced from experimental results. With the help of these rather simple models chemists were able to predict the behavior and the properties of molecules in chemical reactions. This is the reason why they became and still are very popular

in chemistry although do not take the physical laws of quantum mechanics into account.<sup>2–4</sup> The ground breaking heuristic theory of chemical bonding by G. N. Lewis, published more than 90 years ago, suggested the concepts of the octet rule and the electron pair bond<sup>5,6</sup> and was later put on quantum chemical ground by Linus Pauling.<sup>7</sup>

For a complete understanding of the chemical bond, a description of chemical bonding properties should, on the one hand, ground on the fundamental laws of quantum mechanics in order to understand the mechanism of bond formation. On the other hand, the description should provide insight in terms of plausible models to provide easy predictability of chemical behavior. The energy decomposition analyses (EDA) which were developed by Morokuma<sup>8</sup> and by Ziegler and Rauk<sup>9</sup> are powerful methods which bridge the gap between elementary quantum mechanics and a conceptually simple interpretation of the nature of the chemical bond. The EDA decomposes the instantaneous interaction energy  $\Delta E_{\text{int}}$  between two fragments A–B in a molecule A–B into three well-defined terms that can be interpreted in chemically meaningful ways. These terms are (1) the quasiclassical electrostatic interaction energy between the charge densities of the fragments,  $\Delta E_{\text{elstat}}$ , (2) the exchange repulsion between the fragments due to Pauli's principle,  $\Delta E_{\text{Pauli}}$ , and (3) the energy gain due to orbital mixing of the fragments,  $\Delta E_{\text{orb}}$ . The terms are defined by assigning intermediate states of the total system during the course of bond formation which are calculated by applying the laws of quantum mechanics. The definition of the states focuses on the interpretability of the resulting energy terms in a chemical sense. Thus, the EDA provides a bridge between the physical laws of quantum mechanics and the heuristic bonding models of chemistry. In this review, after a short description of the theoretical background of the method, we present illustrative examples of bonding situations using the EDA to demonstrate how it can be used to analyze chemical bonds in molecules and to translate results of quantum chemical calculations into terms like covalency, ionicity, aromaticity, donation and backdonation, or hybridization. Although this review focuses on the use of the EDA, we want to point out that several other methods for bonding analysis are available which are covered by further review articles in this journal. Illustrative examples demonstrating how the EDA can interplay with other tools like the Quantum Theory of Atoms in Molecules (QTAIM)<sup>10</sup> method have recently been published in a review article.<sup>11</sup>

In the updated version of this work, we present applications of the newly developed extension

of the method which combines the EDA partitioning scheme with the Natural Orbital for Chemical Valence (NOCV) method developed by Mitoraj and Michalak.<sup>12</sup> The EDA–NOCV<sup>13</sup> scheme makes it possible to divide the orbital interactions between two interacting species  $\Delta E_{\text{orb}}$  into pairwise contributions of the most relevant MOs. The EDA–NOCV method connects the frontier orbital theory of Fukui<sup>14</sup> and the orbital symmetry rules of Woodward and Hoffmann<sup>15</sup> with a quantitative partitioning of the interaction energy that come from DFT calculations. It is also shown that the calculated values of the orbital term  $\Delta E_{\text{orb}}$  may be used to distinguish between different types of bonding which arise when the fragments are considered in different electronic states.

We wish to point out that, besides the EDA and EDA–NOCV approaches that are described here, several other variants of EDA have been developed in recent years. We do not claim that the Ziegler/Rauk/Mitoraj/Michalak version of the EDA is better than the others. We found it particularly useful, because it provides a consistent decomposition of the energy terms starting from the observable bond dissociation energy up to pairwise orbital interactions that can be graphically displayed. But like all other methods, it may be criticized for its foundation in physical interactions. A truly weak point of the present EDA is, that it can only be used in conjunction with DFT calculations but not with correlated *ab initio* methods. Our general viewpoint is, that molecular models are not right or wrong but more or less useful. Depending on the preference of the author, he/she may prefer to use alternative methods. Here we mention the Block-Localized Wave function (BLW) EDA of Mo<sup>16–20</sup> and the Generalized Product Function (GPF) EDA by Nascimento,<sup>21–23</sup> which are based on Valence Bond (VB) theory. The BLW approach was later extended to DFT calculations.<sup>24</sup> Methods have also been developed which use nonpenetrating charges for calculating Coulombic interactions, such as the Interacting Quantum Atom (IQA) method by Pendás and coworkers<sup>25–29</sup> which is based on the QTAIM approach.<sup>10</sup> A very interesting alternative is the ongoing work by Head-Gordon, who developed methods such as the Absolute Localized Molecular Orbital (ALMO) EDA<sup>30,31</sup> that avoids spin contamination, which is found in overlapping regions of frozen wave functions. Variants have been developed for DFT, HF, and MP2 methods and were applied to a wide variety of chemical problems.<sup>32–37</sup> Furthermore, EDA approaches were introduced by Ruedenberg and Schwartz that

particularly aim at a physical understanding of chemical bonds.<sup>38–40</sup>

The results of the different EDA methods may be very different, because the decomposition procedures are not the same. It is therefore useless to directly compare the numerical values that are provided by the various approaches. More important are the trends, which are suggested for a series of molecules by the EDA approaches. As a rule, the following five criteria should be fulfilled by a quantum chemical method for a bonding analysis:

- Derived from accurate quantum chemical calculations
- Results do not significantly change at different theoretical levels
- Mathematically unambiguously defined
- Plausible interpretation of the different terms
- Useful for chemical problems

It is clear that the last two criteria are subject to personal preferences and that the usefulness of a method may depend on the particular problem. The reason why we have chosen the EDA–NOCV method lies in the comparatively easy approach and the close association with classical bonding models but also with the physical mechanism of the bond formation. In the following we introduce the foundation of the method before we discuss some applications that show the cope but also the limitation of the EDA–NOCV approach.

## THEORETICAL BACKGROUND

The EDA considers the formation of a molecule A–B with the corresponding wave function  $\Psi_{AB}$  and energy  $E_{AB}$  as the result of the interactions between fragments  $A^0$  and  $B^0$  in their electronic and geometric ground states  $\Psi_A^0$  and  $\Psi_B^0$  with energies  $E_A^0$  and  $E_B^0$  which are subdivided into several steps. In a first step, the fragments  $A^0$  and  $B^0$  are distorted from the equilibrium geometries and wave functions  $\Psi_A^0$  and  $\Psi_B^0$  to the geometries and electronic states  $\Psi_A$  and  $\Psi_B$  (with energies  $E_A$  and  $E_B$ ) which they possess in the molecule AB. The total energy that is necessary to distort and electronically excite all fragments to this state is the preparation energy  $\Delta E_{\text{prep}}$  (Eq. (1)):

$$\Delta E_{\text{prep}} = E_A - E_A^0 + E_B - E_B^0 \quad (1)$$

The focus of the EDA lies on the analysis of the instantaneous interaction energy  $\Delta E_{\text{int}}$  which is the

differences between the energy of the molecule  $E_{AB}$  and the energies of the prepared fragments  $E_A$  and  $E_B$  (Eq. (2)):

$$\Delta E_{\text{int}} = E_{AB} - E_A - E_B \quad (2)$$

The bond dissociation energy  $D_e$  is (by definition with opposite sign) then the sum of the instantaneous interaction energy  $\Delta E_{\text{int}}$  and  $\Delta E_{\text{prep}}$  (Eq. (3)):

$$-D_e = \Delta E_{\text{int}} + \Delta E_{\text{prep}} \quad (3)$$

In the first step of the bond formation according to the EDA, the distorted fragments with frozen charge densities A and B are brought from infinite separation to the position in the molecule. This state is the promolecule with the product wave function  $\Psi_A \Psi_B$  and the energy  $E_{AB}^0$ . The interaction between the frozen charges densities of A and B at the equilibrium geometry of AB gives the quasiclassical Coulomb interaction  $\Delta E_{\text{elstat}}$  (Eq. (4)) which is in most cases attractive:

$$\begin{aligned} \Delta E_{\text{elstat}} = & \sum_{\alpha \in A} \sum_{\beta \in B} \frac{Z_\alpha Z_\beta}{R_{\alpha\beta}} + \int dr V_B(r) \rho_A(r) \\ & + \int dr V_A(r) \rho_B(r) + \int \int dr_1 dr_2 \frac{\rho_A(r_1) \rho_B(r_2)}{r_{12}} \end{aligned} \quad (4)$$

In the second step of the EDA, the product wave function  $\Psi_A \Psi_B$  which is normalized but violates the Pauli principle is antisymmetrized and renormalized to give an intermediate state  $\Psi^0$  (Eq. (5)) with the corresponding energy  $E^0$ . The energy difference between  $E_{AB}^0$  and  $E^0$  is termed as exchange (Pauli) repulsion  $\Delta E_{\text{Pauli}}$  (Eq. (6)):

$$\Psi^0 = \overset{\wedge}{N} \{ \Psi_A \Psi_B \} \quad (5)$$

$$\Delta E_{\text{Pauli}} = E_{AB}^0 - E^0 \quad (6)$$

In the third step,  $\Psi^0$  is relaxed to yield the final state  $\Psi_{AB}$  of the molecule A–B with the energy  $E_{AB}$ . The associated energy lowering comes from the orbital mixing and thus, it can be identified as covalent contribution to the chemical bond. It is termed orbital interaction  $\Delta E_{\text{orb}}$  (Eq. (7)):

$$\Delta E_{\text{orb}} = E_{AB} - E_{AB}^0 \quad (7)$$

$\Delta E_{\text{elstat}}$ ,  $\Delta E_{\text{Pauli}}$  and  $\Delta E_{\text{orb}}$  sum up to the total interaction energy  $\Delta E_{\text{int}}$  (Eq. (8)):

$$\Delta E_{\text{int}} = \Delta E_{\text{elstat}} + \Delta E_{\text{Pauli}} + \Delta E_{\text{orb}} \quad (8)$$

It is possible to decompose the orbital interaction  $\Delta E_{\text{orb}}$  into contributions from orbitals which belong to different irreducible representations  $\Gamma$  of the point group of the molecule (Eq. (9)):

$$\Delta E_{\text{orb}} = \sum_{\Gamma} \Delta E_{\Gamma} \quad (9)$$

The  $\Delta E_{\text{orb}}$  term is always attractive as the total wave function is optimized during its calculation. Small repulsive values for contributions of irreducible representations to the total orbital interaction are due to numerical errors in the computation. Large repulsive values for orbital interactions always indicate a wrong setup of the fragments for the EDA calculation. The  $\Delta E_{\text{Pauli}}$  term is always repulsive as additional constraints are added to the wave function. The electrostatic term is usually attractive but in special cases it can yield repulsive contributions (*vide infra*). For a detailed discussion of the theoretical background and general properties of the different contributions to the total interaction energy we refer to the original literature (Refs 8,9) and a detailed review article by F. M. Bickelhaupt and E. J. Baerends.<sup>41</sup>

It is important to realize that the identification of the three major terms  $\Delta E_{\text{elstat}}$ ,  $\Delta E_{\text{Pauli}}$ , and  $\Delta E_{\text{orb}}$  with specific interactions is conceptually attractive but must not be taken as genuine expression of the physical forces. This holds in particular for the term  $\Delta E_{\text{elstat}}$ , which gives the strength of the quasiclassical interactions in A-B between the chosen fragments of A and B using frozen densities. This leads to a penetration of the electronic charges, which means that some electron density close to the nucleus of A belongs to atom B. Methods have also been developed which use nonpenetrating charges for calculating Coulombic interactions, such as the above mentioned IQA method.<sup>25–29</sup> It is obvious that the calculated values for the Coulombic interaction that are given by the IQA method and the EDA-NOCV approach are quite different. There are conflicting views which of the two approaches is physically more reasonable. This is no problem as long as the results are considered as a model.

It has earlier been suggested that the sum of the electrostatic and Pauli terms  $\Delta E_{\text{elstat}}$  and  $\Delta E_{\text{Pauli}}$  may be taken as expression for steric repulsion  $\Delta E_{\text{steric}}$ . But the sum  $\Delta E_{\text{elstat}} + \Delta E_{\text{Pauli}}$  may become attractive in some cases. Steric repulsion can be identified with the Pauli repulsion  $\Delta E_{\text{Pauli}}$  and the discussion of the

interatomic interactions should be made using the three terms  $\Delta E_{\text{elstat}}$ ,  $\Delta E_{\text{Pauli}}$ , and  $\Delta E_{\text{orb}}$  separately. The use of the term  $\Delta E_{\text{steric}} = \Delta E_{\text{elstat}} + \Delta E_{\text{Pauli}}$  is not recommended.

There is one further type of interatomic interactions, which has recently been recognized as an important component of chemical bonding. This is dispersion interaction, which comes from the attractive forces between the induced dipoles of interacting species. Dispersion interaction between one pair is weak, which is the reason that it was often considered to be negligible for chemical bonding. However, if the interacting species are very large, the number of pair interactions grows rapidly and the associated attractive forces may provide an important part of chemical bonding.<sup>42</sup> DFT does not consider dispersion interactions and most functionals were developed without referencing them. If an explicit correction term for dispersion interaction is employed such as in the methods suggested by Grimme,<sup>43,44</sup> the EDA results remain unchanged and the dispersion correction appears as extra term  $\Delta E_{\text{Disper}}$ . If the dispersion interaction is part of the functional it will change the EDA results. Most probably it will yield weaker Pauli repulsion but this needs to be tested. One might consider to combine the sum of dispersion interactions with the Pauli repulsion as a total steric interaction, which could, in principle, become attractive. Since steric interactions in chemistry are usually associated with repulsion, we do not advocate the latter model.

The recently developed EDA-NOCV method<sup>13</sup> combines the EDA with the NOCV approach of Mitoraj and Michalak.<sup>12</sup> The difference between the EDA and the EDA-NOCV methods lies in the expression for the orbital interaction term  $\Delta E_{\text{orb}}$  which is broken down in the EDA-NOCV approach into pairwise contributions of interacting orbitals of the two fragments. The starting point is the deformation density  $\Delta\rho(r)$  which is the difference between the densities of the fragments before and after bond formation. The deformation density  $\Delta\rho(r)$  can be expressed in terms of pairs of complementary eigenfunctions ( $\psi_k \psi_{-k}$ ) with the eigenvalues  $v_k$  and  $v_{-k}$  that possess the same absolute value but opposite sign.

$$\Delta\rho(r) = \sum_k v_k [-\psi_{-k}^2(r) + \psi_k^2(r)] = \sum_k \Delta\rho_k(r) \quad (10)$$

The NOCVs  $\psi_k$  and the associated eigenvalues  $v_k$  are obtained through diagonalization of the difference density matrix  $\Delta P_{\mu\nu}$  of the system.<sup>12</sup> Equation (10)

expresses the total charge deformation  $\Delta\rho(r)$  that is associated with the bond formation in terms of pairwise charge contributions  $\Delta\rho_k(r)$  which come from particular pairs of (NOCV) orbitals. A particularly helpful feature of the EDA–NOCV lies in the graphical display of the individual deformation densities  $\Delta\rho_k(r)$  which provide a pictorial description of the change in the electronic structure that comes from the bond formation.

The total orbital interaction  $\Delta E_{\text{orb}}$  may likewise be derived from pairwise orbital interaction energies  $\Delta E_{\text{orb}}^k$  that are associated with  $\Delta\rho_k(r)$ :

$$\Delta E_{\text{orb}} = \sum_k \Delta E_{\text{orb}}^k = \sum_k v_k \left[ -F_{-k,-k}^{\text{TS}} + F_{k,k}^{\text{TS}} \right] \quad (11)$$

The terms  $F_{-k,-k}^{\text{TS}}$  and  $F_{k,k}^{\text{TS}}$  in Eq. (11) are diagonal transition-state (TS) Kohn–Sham matrix elements corresponding to NOCVs with the eigenvalues  $-v_k$  and  $v_k$ , respectively. Here, the term ‘transition state’ refers to the charge density which is intermediate between the density of the final molecule AB and the superimposed fragment densities of A and B. The  $\Delta E_{\text{orb}}^k$  term of a particular type of bond is assigned by visual inspection of the shape of the deformation density,  $\Delta\rho_k$ . The eigenvalues  $v_k$  are a measure of the size of the densities that is deformed, i.e., accumulated or depleted, along with the orbital interactions.

Experience has shown that the  $\Delta E_{\text{orb}}$  term of the EDA–NOCV has usually only a very small number of significant contributions of  $\Delta E_{\text{orb}}^k$  which makes it possible to identify specific interactions that lead to a chemical bond. This may be used not only to analyze the chemical bond of a molecule but also to investigate the orbital interactions at the transition state. The change in the electron density distribution which comes from bond formation between two fragments or intermolecular interactions during a

chemical reaction can be quantitatively expressed through its energy values  $\Delta E_{\text{orb}}^k$  and the associated the eigenvalues  $v_k$  of the NOCVs.

## BONDING IN MAIN GROUP COMPOUNDS

In this section, we discuss different applications of the EDA on chemical bonding in main group compounds. We will start with a discussion of the chemical bond in simple diatomic molecules which serve as illustrative examples for the numerical results. Next, we show an example of typical donor acceptor bonds that indicates that there are cases where other contributions than orbital interactions can be important to understand trends in bond strength. The last example in the main group part is the presentation of bonding analyses in unsaturated organic molecules illustrating how concepts like aromaticity, conjugation, and hyperconjugation can be unambiguously quantified by the EDA.

### Diatomeric Molecules H<sub>2</sub>, N<sub>2</sub>, CO, and BF

Diatomeric molecules of main-group atoms are often used to introduce standard bonding models of chemistry.<sup>45–47</sup> They are ideal candidates for the explanation of fundamental bonding properties such as covalent bonding,  $\sigma$  and  $\pi$  bonding, ionic character, and so on. For this reason, we start the presentation of properties of the EDA by discussing results of bonding analyses of simple diatomic molecules such as H<sub>2</sub> and N<sub>2</sub> as well as CO and BF which are iso-electronic to N<sub>2</sub>. Table 1 presents the results of EDA investigations of H–H–, N–N–, C–O–, and B–F–bonds. As there is no geometric and electronic preparation of the atomic fragments ( $\Delta E_{\text{prep}} = 0$ ), the

**TABLE 1** | Energy Decomposition Analysis of the H–H, N–N, C–O, and B–F bonds at RPBE/TZP

	H <sub>2</sub>	N <sub>2</sub>	CO	BF
$\Delta E_{\text{int}}$	−112.9	−232.2	−258.4	−180.8
$\Delta E_{\text{Pauli}}$	0.0	791.7	575.8	476.1
$\Delta E_{\text{elstat}}^1$	+5.8	−308.5 (30.1%)	−240.0 (28.8%)	−210.5 (32.0%)
$\Delta E_{\text{orb}}^1$	−118.7 (100%)	−715.4 (69.9%)	−594.2 (71.2%)	−446.4 (68.0%)
$\Delta E_{\sigma}^2$	−118.7 (100%)	−470.0 (65.7%)	−301.7 (50.8%)	−396.4 (88.8%)
$\Delta E_{\pi}^2$	0.0 (0%)	−245.5 (34.3%)	−292.5 (49.2%)	−50.0 (11.2%)
$R^3$	0.745 (0.741)	1.105 (1.09768)	1.144 (1.128)	1.285 (1.262)
$D_0^3$	−106.3 (−103.3)	−228.8 (−225.0)	−255.4 (−255.7)	−178.9 (−179.9)

Taken from Ref 45.

Energy values in kcal/mol, bond length R in Å.

<sup>1</sup> Values in parentheses give the percentage contribution to the total attractive interactions  $\Delta E_{\text{elstat}} + \Delta E_{\text{orb}}$ .

<sup>2</sup> Values in parentheses give the percentage contribution to the orbital interactions  $\Delta E_{\text{orb}}$ .

<sup>3</sup> Experimental values given in parentheses.

interaction energy and the dissociation energy are identical in these molecules.

The EDA shows that  $H_2$  has only one stabilizing contribution to the total interaction energy, i.e., the orbital interactions  $\Delta E_{\text{orb}}$ . The Pauli repulsion  $\Delta E_{\text{Pauli}}$  is zero as there are only two electrons in  $H_2$  having different spin. The electrostatic interaction  $\Delta E_{\text{elstat}}$  at the equilibrium distance is slightly repulsive (+5.8 kcal/mol). We want to point out that  $\Delta E_{\text{elstat}}$  becomes slightly negative at longer distances with an energy minimum at ~10 kcal/mol and a bond length which is significantly longer than the correct value. It has already been shown by Heitler and London that a purely electrostatic description of the interatomic interactions in  $H_2$  yields only a shallow energy minimum at a too long bond.<sup>1</sup>

The bonding picture of  $N_2$  is very different from that of  $H_2$  (see Table 1). The total interaction energy of -232.2 kcal/mol comprises strongly attractive electrostatic and orbital interactions and a large Pauli repulsion of 791.7 kcal/mol. The latter term even overcompensates the orbital stabilization of -715.4 kcal/mol. Without the attractive contributions of -308.5 kcal/mol arising from quasiclassical electrostatic interactions,  $N_2$  would not be stable. The decomposition of the orbital interaction shows that 65.7% (-470.0 kcal/mol) come from the  $\sigma$  bond while 34.3% (-245.4 kcal/mol) come from the two  $\pi$  bonds.

The bond dissociation energy of CO is larger than that of  $N_2$ . The EDA shows that the increase does not come from stronger electrostatic or orbital attraction but from weaker Pauli repulsion. Stronger bonds may thus come not only from an increase of attraction but from a decrease of repulsion. Note that the relative contributions of the  $\pi$  bonds to the total orbital interactions in CO (49.2%) are larger than in  $N_2$  (34.3%) which means that CO has clearly triple-bond character. BF has the smallest bond dissociation energy in the series of the isoelectronic molecules  $N_2$ , CO, and BF. Although the Pauli repulsion is even smaller than in CO, this loss of repulsion does not compensate for the decrease of  $\Delta E_{\text{elstat}}$  and  $\Delta E_{\text{orb}}$ . While both the total and the relative contributions of the  $\sigma$  bond to the total  $\Delta E_{\text{orb}}$  in BF are larger than those in CO they are overcompensated by a drastic loss of  $\pi$  bonding energy (-50.0 kcal/mol in BF vs -292.5 kcal/mol in CO). This is in agreement with the classical Lewis picture of BF with only a B–F single bond supported by donation of electron lone-pairs at fluorine into vacant orbitals at boron but not by  $\pi$  bonding.

The comparison of  $N_2$ , CO, and BF shows that a detailed inspection of all individual terms of the total interaction energy is necessary to understand the strength and the nature of a chemical bond. The

EDA reveals that  $\Delta E_{\text{elstat}}$  strongly contributes to the chemical bonding even in case of nonpolar bonds. A systematic study of 184 diatomic molecules has shown that electrostatic interactions are very important for the chemical bonds in nearly all molecules.<sup>48</sup> A notable exception is the bonding in  $H_2$ . Covalent bonding is introduced in elementary courses of chemistry and in many textbooks because the effect of orbital interactions can be easily demonstrated. However,  $H_2$  is atypical for chemical bonds for two reasons. One reason is the absence of Pauli repulsion which plays an important role for nearly all chemical bonds.<sup>45–47</sup> The second reason is the small nucleus of the hydrogen atoms which yield a relatively weak electrostatic attraction compared with heavier nuclei. The very large value for  $\Delta E_{\text{elstat}}$  in  $N_2$  comes from the nuclei of the nitrogen atoms which carry a much higher positive charge than hydrogen.

### Polar Single Bonds in $X_3B-EH_3$ ( $X = H, Cl; E = N, P$ )

In this section, we discuss properties of donor-acceptor B–N- and B–P-bonds between classical Lewis acids and bases and the influence of the substituents at the boron atom.<sup>49,50</sup> The selected examples which we present illustrate the insight into the nature of the chemical bond in typical donor–acceptor complexes. More examples can be found in a review.<sup>51</sup> Table 2 gives EDA results of B–N- and B–P-bonds in  $H_3B-NH_3$ ,  $Cl_3B-NH_3$ ,  $H_3B-PH_3$ , and  $Cl_3B-PH_3$ .

Substitution of hydrogen by chlorine at the boron atom lowers both  $-D_e$  and  $\Delta E_{\text{int}}$ , the same holds for the substitution of nitrogen by phosphorous. Note, that in the presented compounds, the  $\Delta E_{\text{prep}}$  values exhibit significant differences (e.g., 12.7 kcal/mol in  $H_3B-NH_3$  vs 21.5 kcal/mol in  $Cl_3B-NH_3$ ). The distortion of the  $BCl_3$  fragment from the planar minimum geometry to the pyramidal structure in the complex needs more energy than that of  $BH_3$ , as the donation of electron density into the vacant p orbital at the boron atom stabilizes the planar geometry of  $BCl_3$ . Due to the differences in the preparation energy the bond dissociation energy is not a good probe to estimate the intrinsic donor–acceptor strength in these compounds. Only the interaction energy can provide inside into the donor–acceptor interaction. What is the reason for the decrease of total interaction energy of the Lewis bases to  $BCl_3$  compared to  $BH_3$ ? The results of the EDAs of the B–N-bonds indicate that both, the attractive electrostatic and orbital interactions, are larger for compounds with  $BCl_3$ . This is overcompensated by a drastic increase of the Pauli repulsion because of the

**TABLE 2** | Energy Decomposition Analysis of the Boron–Amine- and Boron–Phosphane Complexes  $X_3B-EH_3$  ( $X = H, Cl; E = N, P$ ) Bonds at BP86/TZ2P

	$H_3B-NH_3$	$Cl_3B-NH_3$	$H_3B-PH_3$	$Cl_3B-PH_3$
$\Delta E_{int}$	-44.6	-41.3	-38.6	-25.1
$\Delta E_{Pauli}$	108.8	192.8	113.3	166.4
$\Delta E_{elstat}^1$	-77.3 (50.4%)	-120.5 (51.5%)	-58.0 (38.2%)	-89.6 (46.1%)
$\Delta E_{orb}^1$	-76.0 (49.6%)	-113.6 (48.5%)	-93.9 (61.8%)	-104.7 (53.8%)
$\Delta E_{\sigma}(a_1)^2$	-68.4 (89.9%)	-102.2 (89.9%)	-79.3 (84.6%)	-92.0 (87.8%)
$\Delta E(a_2)^2$	0.0 (0.0%)	-0.2 (0.2%)	0.0 (0.0%)	-0.1 (0.1%)
$\Delta E_{\pi}(e_1)^2$	-7.7 (10.1%)	-11.3 (9.9%)	-14.7 (15.6%)	-12.6 (12.1%)
$\Delta E_{prep}$	12.7	21.5	12.2	23.0
$-D_e$	-31.9	-19.8	-26.4	-2.1
$R$	1.657	1.633	1.939	2.026

Taken from Refs 49 and 50.

Energy values in kcal/mol, Bond Length  $R$  in Å.

<sup>1</sup> Values in parentheses give the percentage contribution to the total attractive interactions  $\Delta E_{elstat} + \Delta E_{orb}$ .

<sup>2</sup> Values in parentheses give the percentage contribution to the orbital interactions  $\Delta E_{orb}$ .

larger electron density at the boron atom in  $Cl_3B-EH_3$  due to electron donation from the chlorine atoms. Note that the B–N-bond length in  $H_3B-NH_3$  is larger than that in  $Cl_3B-NH_3$ . Thus the bond length does not correlate with the bond strength in this case, neither in terms of dissociation energies nor in terms of interaction energies.

To investigate the effect of the Lewis base atom (N vs P) we compare the EDA results of  $H_3B-NH_3$  with those of  $H_3B-PH_3$ . The interaction energy of the B–P bond is smaller than that of the B–N-bond (-38.6 kcal/mol vs -44.6 kcal/mol). While absolute and also relative orbital contributions are larger in the phosphorous complex, weaker electrostatic interactions, and slightly larger Pauli repulsion result in the slightly weaker bond strength. A comparison of  $Cl_3B-NH_3$  with  $Cl_3B-PH_3$  shows, that in this case the smaller interaction energy in the phosphorous compound (-25.1 kcal/mol vs -41.3 kcal/mol) comes mainly from the weak electrostatic interactions (-89.6 kcal/mol vs -120.5 kcal/mol in  $Cl_3B-NH_3$ ).

## Strength of Conjugation and Aromaticity

Conjugation and aromaticity are terms used to discuss the stability of unsaturated acyclic and cyclic compounds.<sup>52–54</sup> The structure and the reactivity of many compounds which possess  $\pi$  bonds are often explained in terms of aromaticity or conjugative stabilization. Conjugation and aromaticity are frequently accounted for by invoking by  $\pi-\pi^*$  interactions. It was as early as 1931 when the phenomenon of aromaticity was put on a quantum chemical ground by Erich Hückel<sup>55–58</sup> for the first time (these studies were later summarized to the

famous  $4n + 2$  formula by von Doering<sup>59</sup>). However, aromaticity and conjugation are no physical observables but terms of chemical models. A quantification of these effects is usually done by comparison to more or less arbitrarily chosen reference systems and thus are a permanent matter of controversy.<sup>60,61</sup> Due to their large importance on chemistry, one of us (GF) put the terms ‘aromaticity’ and ‘conjugation’ into the group of the ‘many unicorns in the world of chemical bonding models’,<sup>4</sup> as every chemists knows how they look like although nobody has ever seen them. In this part we will demonstrate how the EDA can be used to quantify the effects of conjugation and aromaticity.

Table 3 presents the results of EDA studies on unsaturated hydrocarbons 1,3-butadiyne, 1,3-butadiene, and 1,3,5-hexatriene and the two saturated molecules ethane and 2,2,3,3-tetramethylbutane. The fragments were chosen such that a C–C single bond was broken homolytically (see Table 3). As the single-bond has  $\sigma$  symmetry, the  $\pi$  orbital  $\Delta E_{\pi}$  contributions to the orbital interactions are a measure for the conjugative stabilization.

From the  $\Delta E_{\pi}$  contributions it becomes obvious that two conjugated triple bonds in 1,3-butadiyne result in larger conjugative stabilization (-45.0 kcal/mol) than the conjugated double bonds in 1,3-butadiene (-19.5 kcal/mol) or in 1,3,5-hexatriene (-22.0 kcal/mol). The latter two values show that a longer chain of conjugated double bonds yields larger conjugative stabilization of the C–C-single bonds. This finding is in line with the shorter C–C distances which correlate with the conjugative stabilization in these three unsaturated hydrocarbons. The

**TABLE 3** | EDA Results of C–C-Single Bonds in Different Hydrocarbons at BP86/TZ2P

$\Delta E_{\text{int}}$	-176.0	-128.5	-132.1	-114.8	-93.2
$\Delta E_{\text{Pauli}}$	161.8	268.4	271.3	200.8	253.6
$\Delta E_{\text{elstat}}^1$	-114.6 (33.9%)	-169.9 (42.8%)	-172.4 (42.7%)	-131.3 (41.6%)	-163.5 (47.2%)
$\Delta E_{\text{orb}}^1$	-223.3 (66.1%)	-227.0 (57.2%)	-231.1 (57.3%)	-184.2 (58.4%)	-183.2 (52.8%)
$\Delta E_{\sigma}^2$	-178.3 (79.8%)	-207.5 (91.4%)	-209.0 (90.5%)	-174.3 (94.6%)	-171.0 (93.3%)
$\Delta E_{\pi}^2$	-45.0 (20.2%)	-19.5 (8.8%)	-22.0 (9.5%)	-10.0 (5.4%)	-11.6 (6.4%)
$\Delta E_{\text{prep}}$	5.4	13.0	13.4	21.8	30.2
$-D_e$	-170.6	-115.5	-118.7	-93.0	-63.0
$R(\text{C}-\text{C})$	1.361	1.453	1.444	1.532	1.591

Values taken from Refs 52 and 53.

Energies in kcal/mol.

<sup>1</sup> Values in parentheses give the percentage contribution to the total attractive interactions  $\Delta E_{\text{elstat}} + \Delta E_{\text{orb}}$ .

<sup>2</sup> Values in parentheses give the percentage contribution to the orbital interactions  $\Delta E_{\text{orb}}$ .

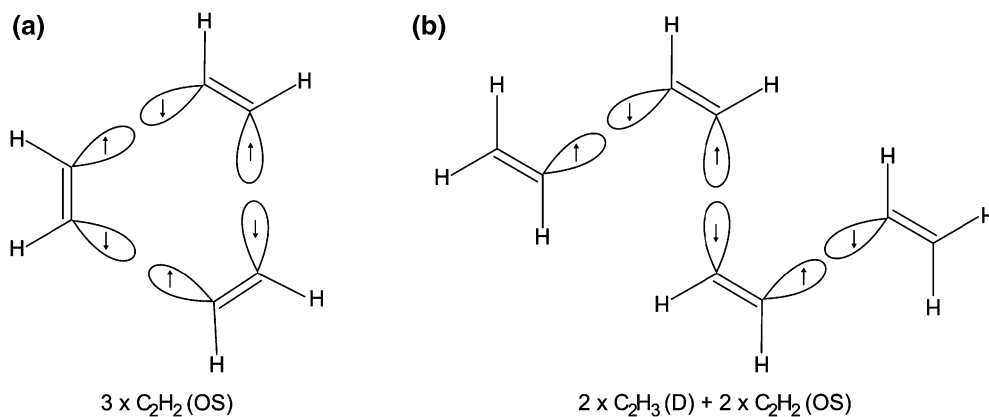
hyperconjugation effect of methyl groups in saturated hydrocarbons is revealed by comparing ethane with 2,2,3,3-tetramethylbutane. Although the C–C-bond distance of the latter molecule is larger and the interaction energy is smaller, the  $\pi$ -type contributions are slightly bigger (-11.6 kcal/mol) than in ethane (-10.0 kcal/mol).

While conjugation can be quantified with the EDA by analyzing the intrinsic energy contributions, proper reference systems have to be chosen for a measurement of the aromatic stabilization energy (ASE) in cyclic unsaturated compounds. A popular approach to an energy based quantification of aromaticity is the comparison of heats of hydrogenation reactions of double bonds. This is a questionable approach because the reactions do not only imply changes in the  $\pi$  bonding but in all chemical bonds of the system.<sup>62</sup> With the help of the EDA, the aromatic stabilization energies (ASE) can be directly computed by comparing the total amount of conjugative

stabilization of single bonds in cyclic unsaturated systems with that amount in acyclic systems with the same number of single bonds (Scheme 1).

This approach is demonstrated in Table 4 for a comparison of benzene and five heterocyclic 6 $\pi$  species  $C_5H_5X$  ( $X = N, P, As, Sb, Bi$ ) with the related acyclic molecules.

Benzene was homolytically fragmented into three  $C_2H_2$  fragments in open shell singlet states. It does not matter that the latter species possess broken-symmetry because the relevant term concerns the relaxation of the  $\pi$ -orbitals which are not affected by the symmetry of the  $\sigma$  frame. The corresponding acyclic reference system with three homolytically cleaved C–C-single bonds is 1,3,5,7-octatetraene with two  $C_2H_3$  fragments in doublet states and two  $C_2H_2$  fragments in open shell singlet states (Scheme 1). Note that, although this system includes more  $\pi$  electrons (8 instead of 6 in benzene), it includes three C–C-interactions as in benzene. The total  $\pi$

**SCHEME 1** | Fragments which are used for the EDA (a) of benzene and (b) 1,3,5,7-octatetraene. D, doublet; OS, open shell singlet.

**TABLE 4** | EDA Results of Benzene and Group 5 Heterobenzenes and Acyclic Reference Systems at BP86/TZ2P. Energies in kcal/mol. Aromatic Stabilization Energies (ASE) Were Computed from the Difference of  $\Delta E_{\pi}$  in the Cyclic and the Acyclic Compound

X	CH	N	P	As	Sb	Bi
$\Delta E_{\text{int}}$	-513.3	-495.0	-464.7	-453.2	-440.0	-431.5
$\Delta E_{\text{Pauli}}$	1180.0	1356.2	1169.9	1120.4	1070.5	1044.0
$\Delta E_{\text{elstat}}^1$	-540.4 (31.9%)	-563.0 (30.4%)	-517.1 (31.6%)	-504.1 (32.0%)	-489.2 (32.4%)	-478.0 (32.5%)
$\Delta E_{\text{orb}}^1$	-1152.8 (68.1%)	-1288.2 (69.6%)	-1117.5 (68.4%)	-1069.4 (68.0%)	-1021.3 (67.6%)	-995.5 (67.5%)
$\Delta E_{\sigma}^2$	-1045.2 (90.7%)	-1174.7 (91.2%)	-1016.2 (90.9%)	-971.6 (90.8%)	-926.5 (90.7%)	-901.9 (90.6%)
$\Delta E_{\pi}^2$	-107.7 (9.3%)	-113.5 (8.8%)	-101.3 (9.1%)	-97.8 (9.2%)	-94.8 (9.3%)	-93.6 (9.4%)
ASE	42.5	45.7	36.9	34.9	31.1	29.4

X	CH	N	P	As	Sb	Bi
$\Delta E_{\text{int}}$	-489.5	-456.0	-426.0	-415.4	-404.4	-397.2
$\Delta E_{\text{Pauli}}$	1064.9	1194.9	993.6	955.5	923.4	906.6
$\Delta E_{\text{elstat}}^1$	-512.5 (33.0%)	-565.5 (34.2%)	-502.2 (35.4%)	-484.9 (35.4%)	-471.4 (35.5%)	-461.2 (35.4%)
$\Delta E_{\text{orb}}^1$	-1041.9 (67.0%)	-1085.4 (65.8%)	-917.4 (64.6%)	-886.0 (64.6%)	-856.5 (64.5%)	-842.6 (64.6%)
$\Delta E_{\sigma}^2$	-976.7 (93.7%)	-1017.5 (93.8%)	-853.0 (93.0%)	-823.1 (92.9%)	-792.8 (92.6%)	-778.5 (92.4%)
$\Delta E_{\pi}^2$	-65.2 (6.3%)	-67.8 (6.2%)	-64.4 (7.0%)	-62.9 (7.1%)	-63.7 (7.4%)	-64.2 (7.6%)

Values taken from Ref 54.

<sup>1</sup> Values in parentheses give the percentage contribution to the total attractive interactions  $\Delta E_{\text{elstat}} + \Delta E_{\text{orb}}$ .

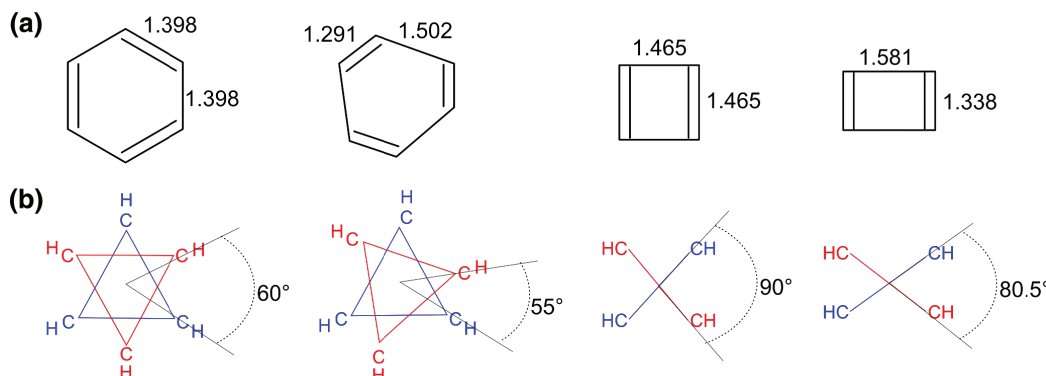
<sup>2</sup> Values in parentheses give the percentage contribution to the orbital interactions  $\Delta E_{\text{orb}}$ .

contributions to the orbital interactions are -107.7 kcal/mol in benzene and -65.2 kcal/mol in 1,3,5,7-octatetrene. Thus the difference of an acyclic and a cyclic system for a stabilization of the three C–C-single bonds that are implied by the latter fragmentation is 42.5 kcal/mol which is the ASE for benzene according to the EDA.

The same comparison for the heteroaromatic compounds suggests, that the ASE in pyridine (45.7 kcal/mol) is even slightly larger than in benzene, while the ASE decreases by going to the larger homologues X (36.9 kcal/mol for X = P, 29.4 kcal/mol for X = Bi). Similar studies on cyclobutadiene give a large negative ASE.<sup>54</sup> The EDA was also employed to estimate the strength of aromaticity in metallabenzenes.<sup>63</sup> Analyses of osma-, ruthena-, irida-, rhoda-, platina-, and palladabenzenes which possess 16 or 18 valence electrons on the metal center indicate that these compounds are 10 $\pi$  aromatic systems where stabilization due to aromatic conjugation is smaller than in benzene.<sup>64</sup>

While the approach discussed so far focuses on the calculation of the stabilization of the  $\pi$  system due to aromaticity, Pierrefixe, and Bickelhaupt presented a different fragmentation pattern for a further analysis of the nature of aromaticity and antiaromaticity with the EDA<sup>65,66</sup>: In benzene, the first, third, and fifth CH group are treated as one fragment and the second, fourth, and sixth CH group are the second fragment resulting in two fragments each forming a regular triangle (Scheme 2).

Each fragment has nine unpaired electrons, six  $\sigma$  type and three  $\pi$  type. In this case the interaction energy covers the bond formation of all  $\sigma$  and  $\pi$  bonds. By rotating the two fragments with respect to each other it is possible to study the effect of geometrical distortion from a localized molecule, having three shorter C–C double bonds and three longer C–C single bonds to the delocalized structure with six equal C–C bond distances. The same analysis is done with cyclobutadiene for comparison (Scheme 2). The result of this analysis is that in



**SCHEME 2 |** (a) Equilibrium geometries of benzene and cyclobutadiene and distorted geometries which were used in the EDA calculations in Ref 65. (b) Schematic representation of the two fragments (colored in red and blue) which were used for the EDA calculations in Ref 65.

both cases, the  $\sigma$  stabilization strongly increases by bringing the molecule from the localized structure to the delocalized one while the  $\pi$  stabilization decreases. In the case of the antiaromatic cyclobutadiene, the destabilization of the  $\pi$  system is so large that it overcompensates the gain of  $\sigma$  interaction upon delocalization and thus, it prevents cyclobutadiene from becoming delocalized. In contrast, in the aromatic system benzene the decrease of  $\pi$  interaction upon forming the delocalized structure is much less so that the delocalized structure is formed. This finding is in agreement with the previous report by Shaik and Hiberty<sup>67</sup> who showed using a Valence Bond approach that it is the  $\sigma$  frame which causes the delocalized structure with equal bond length. The same conclusion was made by Fernandez and Frenking<sup>54</sup> with the EDA where  $\sigma$  and  $\pi$  interactions between six CH fragments were calculated for benzene with (1)  $D_{6h}$  equilibrium geometry and (2)  $D_{3h}$  geometry which has three long and three short C–C bonds. The comparison of the  $\Delta E_\pi$  contributions to the total orbital interactions  $\Delta E_{\text{orb}}$  shows that the  $\pi$  bonding in the  $D_{3h}$  structure is stronger than in the  $D_{6h}$  equilibrium form. The latter geometry is favored over the former because of the stronger  $\Delta E_\sigma$  contributions and because of the larger electrostatic interactions.

## BONDING IN TRANSITION METAL COMPOUNDS

In this section, we discuss different bonding patterns in transition metal compounds featuring selected examples of metal–ligand bonds. Further examples can be found in a review.<sup>51</sup> We start with a comparison of the metal–carbonyl bond with other metal–ligand interactions. Next we show differences

between the bonding situation of ferrocene and bis(benzene)chromium. In the last part we will demonstrate how the EDA can be applied to derive a plausible bonding model for the description of the highly coordinated compound  $[\text{Mo}(\text{ZnCp}^*)_3(\text{ZnMe})_9]$  that has recently been synthesized.

## Transition Metal–Ligand Interactions in $(\text{CO})_5\text{W-L}$ ( $\text{L} = \text{CO, BF, nNHC, aNHC, IMID, C}_2\text{H}_2, \text{C}_2\text{H}_4, \text{PMe}_3, \text{PF}_3, \text{and PCl}_3$ )

Carbonyl compounds are useful reference systems for the discussion of metal–ligand bonding in transition metal complexes.<sup>68–71</sup> The interactions between a transition metal center and a ligand are often explained in terms of the Dewar–Chatt–Duncanson (DCD) model.<sup>72–75</sup> In this model, the bond is formed by a  $\sigma$  donation from the ligand to a vacant acceptor orbital at the transition metal and a  $\pi$  backdonation into a vacant—usually antibonding—orbital at the ligand. In the case of the carbonyl complexes, the  $\sigma$  donation comes from the HOMO of the CO, which is a  $\sigma$  orbital with larger coefficients at the carbon atom. There are two contributions of  $\pi$  backdonation, one into each of the two  $\pi^*$  orbitals of the CO-ligand (see Figure 1(a) and (b)). In the case of unsaturated hydrocarbons which are bonded as  $\eta^2$  ligands, the  $\sigma$  donation comes from the C–C in-plane  $\pi_{||}$  bond of the ligand and  $\pi$  backdonation is into the corresponding C–C  $\pi^*$  orbital (Figure 1(c) and (d)). With an acetylene ligand, additional out-of-plane  $\pi_{\perp}$  donation and  $\delta$  backdonation from the C–C– $\pi$ -bond perpendicular to the TM–C–C-plane are possible (Figure 1(e) and (f)). With singlet carbenes as ligands, the  $\sigma$  donation comes from the  $\sigma$  lone-pair orbital at the carbene center which is usually the HOMO while the  $\pi$  backdonation accumulates electron density into a vacant orbital that is usually

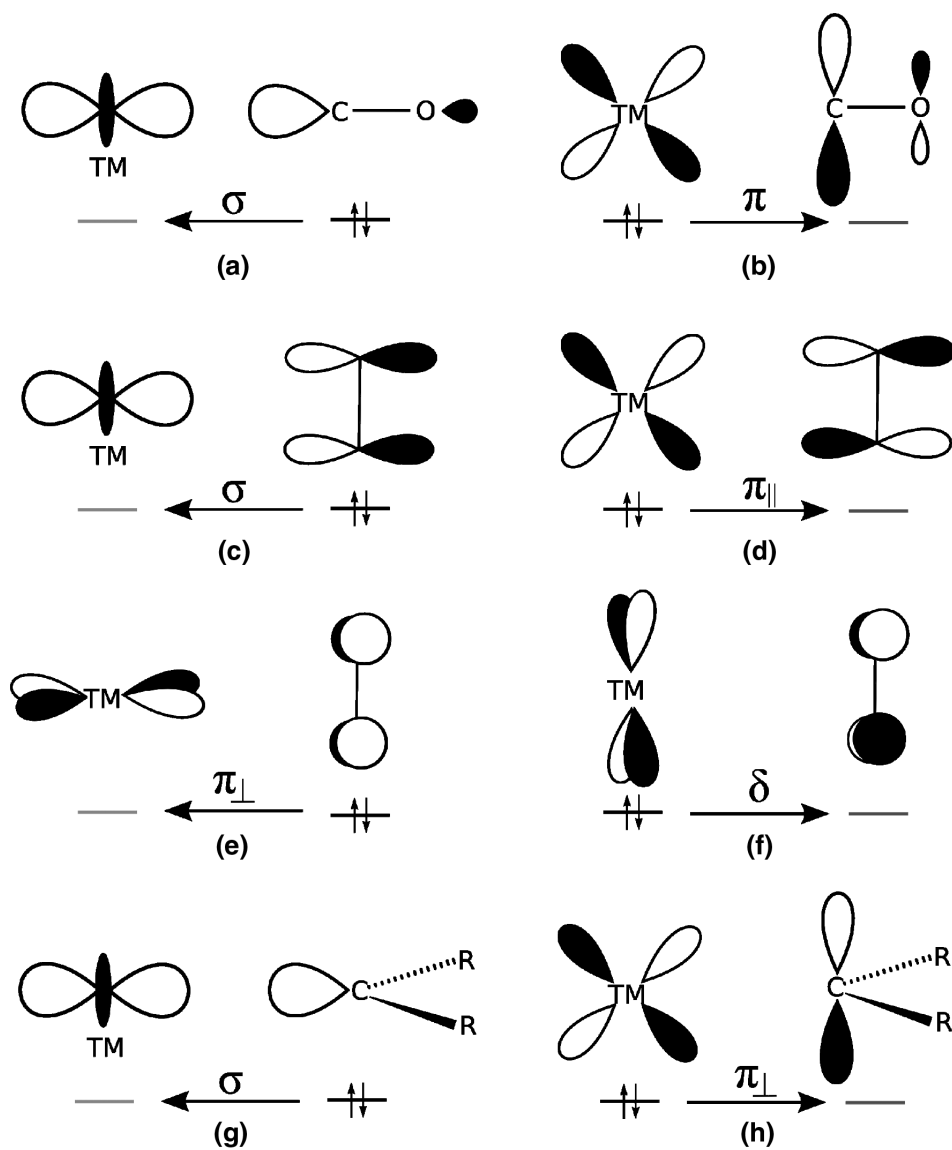


**FIGURE 1** | Schematic representations of interactions according to the Dewar–Chatt–Duncanson model. (a) and (b):  $\sigma$  donation and  $\pi$ -backdonation in an interaction between a transition metal (TM) and a carbonyl (CO); (c) and (d):  $\sigma$  donation and  $\pi$  backdonation in an interaction between a TM and a C=C double- or triple bond; (e) and (f): additional possible contributions of  $\pi$  donation and  $\delta$  backdonation in the interaction between a TM and a C=C-triple bond; (g) and (h):  $\sigma$  donation and  $\pi$  backdonation in singlet carbene complexes.

associated with the empty p atomic orbital of the carbene center (Figure 1(g) and (h)).

The EDA allows to quantify the contributions of each term of donation and backdonation in transition metal complexes and also allows to justify if the DCD model is appropriate for a description of metal–ligand bonds. The DCD model considers only orbital interactions but no quasiclassical electrostatic attraction or Pauli repulsion. The latter terms are given by the EDA calculations. Examination of the trend of all three terms makes it possible to see if the overall trend is indeed determined by  $\Delta E_{\text{orb}}$  only.

Table 5 shows EDA results for the interactions between a  $(\text{CO})_5\text{W}$  fragment in its electronic singlet ground state with CO, isoelectronic BF and the unsaturated hydrocarbons acetylene ( $\text{C}_2\text{H}_2$ ) and ethylene ( $\text{C}_2\text{H}_4$ ). Table 6 gives EDA results for the interactions between  $(\text{CO})_5\text{W}$  with the ligands imidazole (IMID) and its two tautomers imidazol-2-ylidene (nNHC, normal N-heterocyclic carbene) and imidazol-4-ylidene (aNHC, abnormal N-heterocyclic carbene, see Scheme 3). Table 7 gives the EDA results between the interactions of  $\text{W}(\text{CO})_5$  with three phosphine ligands  $\text{PMe}_3$ ,  $\text{PF}_3$ , and  $\text{PCl}_3$ .

**TABLE 5** | EDA Results for the Complexes  $(CO)_5W-L$  ( $L = CO, BF, C_2H_2$ , and  $C_2H_4$ ) at BP86/TZ2P

	$(CO)_5W-CO^1$	$(CO)_5W-BF^1$	$(CO)_5W-(C_2H_2)$	$(CO)_5W-(C_2H_4)$
$\Delta E_{int}$	-49.7	-67.0	-38.1	-35.4
$\Delta E_{Pauli}$	118.6	165.5	103.5	93.0
$\Delta E_{elstat}^2$	-89.6 (53.3%)	-141.6 (60.9%)	-75.0 (52.9%)	-70.0 (54.5%)
$\Delta E_{orb}^2$	-78.6 (46.7%)	-90.9 (39.1%)	-66.6 (47.1%)	-58.4 (45.5%)
$\Delta E(\sigma)^3$	-36.3 (46.1%)	-49.7 (54.6%)	-28.4 (42.6%)	-28.8 (49.3%)
$\Delta E(\pi_{  })^3$	-42.3 (53.9%)	-41.2 (45.3%)	-32.8 (49.2%)	-26.2 (44.9%)
$\Delta E(\pi_{\perp})^3$	—	—	-4.1 (6.1%)	-2.7 (4.6%)
$\Delta E(\delta)^3$	—	—	-1.4 (2.1%)	-0.7 (1.3%)
$\Delta E_{prep}$	4.0	4.3	11.6	7.5
$-D_e$	-45.7	-62.7	-26.6	-27.9

Taken from Ref 69.

Energy values in kcal/mol.

<sup>1</sup> Previously unpublished results. EDA for  $(CO)_5W-CO$  at BP86/TZP (a slightly smaller basis set) give similar results (see Ref 68).

<sup>2</sup> Values in parentheses give the percentage contribution to the total attractive interactions  $\Delta E_{elstat} + \Delta E_{orb}$ .

<sup>3</sup> Values in parentheses give the percentage contribution to the orbital interactions  $\Delta E_{orb}$ .

The results in Table 5 show that CO is more weakly bonded to  $W(CO)_5$  than BF. This holds equally for the bond dissociation energy  $D_e$  and for the interaction energy  $\Delta E_{int}$  because the preparation energies  $\Delta E_{prep}$  for  $(CO)_5W-CO$  and  $(CO)_5W-BF$  are nearly the same. The much stronger  $(CO)_5W-BF$  bond shows that the bond strength is not a sufficient criterion for a compound to become synthesized. Examination of the individual terms of the EDA suggests that the stronger bond in  $(CO)_5W-BF$  compared with isoelectronic  $(CO)_5W-CO$  comes mainly from the larger electrostatic attraction rather than from stronger orbital interactions. The  $\Delta E_{elstat}$  value in the former compound (-141.6 kcal/mol) is 52.0 kcal/mol bigger than in the latter (-89.6 kcal/mol) while the  $\Delta E_{orb}$  value in  $(CO)_5W-BF$  (-90.9 kcal/mol) is only 12.3 kcal/mol larger than in  $(CO)_5W-CO$  (-78.6 kcal/mol). Accordingly, the  $(CO)_5W-BF$  bond has a higher electrostatic character (60.9%) than the  $(CO)_5W-CO$  bond (53.3%). The Pauli repulsion in  $(CO)_5W-BF$  is significantly stronger (165.5 kcal/mol) than in  $(CO)_5W-CO$  (118.6 kcal/mol) which shows that the strengthening in the former bond comes from the attractive terms.

The calculated EDA terms for the chemical bonding in  $(CO)_5W-(C_2H_2)$  and  $(CO)_5W-(C_2H_4)$  reveal that the slightly higher bond dissociation energy  $D_e$  of the latter complex comes from the smaller preparation energy  $\Delta E_{prep}$  rather than from the strength of intrinsic strength of the metal-ligand interactions. The  $\Delta E_{prep}$  value for  $(CO)_5W-(C_2H_4)$  (7.5 kcal/mol) is 4.1 kcal/mol smaller than for  $(CO)_5W-(C_2H_2)$  (11.6 kcal/mol) which overcompensates the slightly stronger  $\Delta E_{int}$  value for

$(CO)_5W-(C_2H_2)$  (-38.1 kcal/mol) compared with  $(CO)_5W-(C_2H_4)$  (-35.4 kcal/mol). The calculated data suggest that the bond dissociation energy can be misleading for estimating the relative strengths of metal-ligand bonds. A further examination of the EDA values for  $(CO)_5W-(C_2H_2)$  and  $(CO)_5W-(C_2H_4)$  indicates that the slightly stronger interactions in the former complex ( $\Delta \Delta E_{int} = 2.7$  kcal/mol) nicely correlate with the contributions which come from the second  $\pi$  orbital of the acetylene ligand. The  $\pi_{\perp}$  donation (-4.1 kcal/mol) and  $\delta$  back donation (-1.4 kcal/mol) in  $(CO)_5W-(C_2H_2)$  are 2.1 kcal/mol stronger than in  $(CO)_5W-(C_2H_4)$ . One might therefore argue that the stronger metal-ligand interactions in the former bond come from the second  $\pi$  orbital of the acetylene ligand. Such reasoning implies, however, that the differences of the remaining energy terms for the metal-ligand interactions between  $(CO)_5W-(C_2H_2)$  and  $(CO)_5W-(C_2H_4)$  cancel. Note that this is numerically correct but conceptually arbitrary. One might equally take the stronger electrostatic attraction in  $(CO)_5W-(C_2H_2)$  (-75.0 kcal/mol) compared with  $(CO)_5W-(C_2H_4)$  (-70.0 kcal/mol) as explanation for the stronger bond of the acetylene ligand. What comes clearly to the fore by the EDA is the finding that acetylene is a 2-electron but not a 4-electron donor ligand, because the contributions from the  $\pi_{\perp}$  donation and  $\delta$  back donation are much weaker than the  $\pi_{||}$  interactions.

Table 6 presents EDA results of  $(CO)_5W$  complexes with the tautomeric ligands ‘normal’ N-heterocyclic carbene (nNHC), ‘abnormal’ N-heterocyclic carbene (aNHC), and imidazol (IMID) (see Scheme 3).

**TABLE 6** | EDA Results for Compounds  $(CO)_5W-L$  ( $L = nNHC$ ,  $aNHC$  and IMID)

	$(CO)_5W-nNHC^1$	$(CO)_5W-aNHC^1$	$(CO)_5W-IMID^1$
$\Delta E_{int}$	-58.3	-62.1	-36.6
$\Delta E_{Pauli}$	124.3	126.0	69.2
$\Delta E_{elstat}^2$	-129.1 (70.7%)	-133.5 (70.9%)	-72.1 (68.1%)
$\Delta E_{orb}^2$	-53.5 (29.3%)	-54.7 (29.1%)	-33.7 (31.9%)
$\Delta E(\sigma)^3$	-43.5 (81.3%)	-45.6 (83.4%)	-27.7 (82.0%)
$\Delta E(\pi_\perp)^3$	-10.0 (18.7%)	-9.1 (16.6%)	-6.1 (18.0%)
$\Delta E_{prep}$	2.2	2.0	1.5
$-D_e$	-55.7	-59.6	-35.1

Taken from Ref 70.

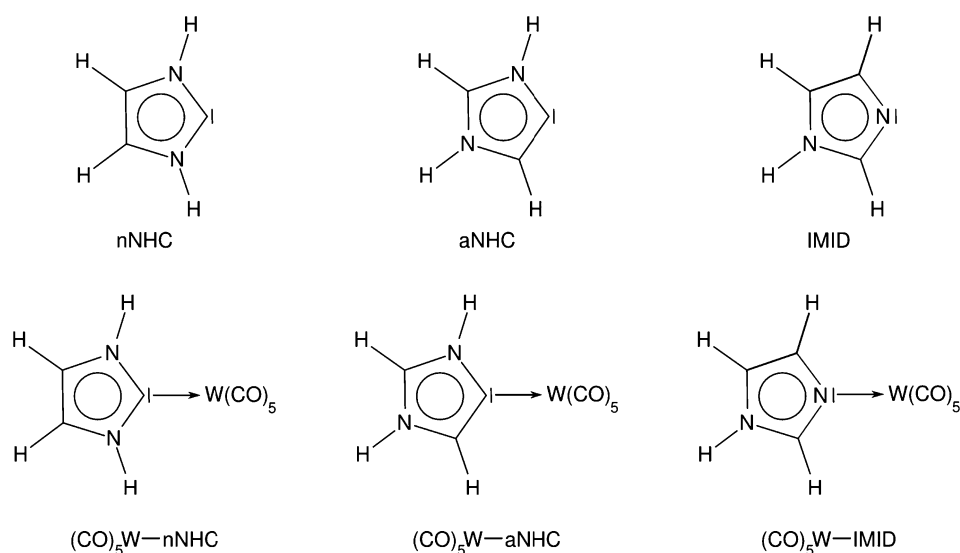
Energy values in kcal/mol.

<sup>1</sup> nNHC, imidazol-2-ylidene (normal N-heterocyclic carbene); aNHC, imidazol-4-ylidene (abnormal N-heterocyclic carbene); IMID, imidazole; see Scheme 3 for graphical representations of the ligands.<sup>2</sup> Values in parentheses give the percentage contribution to the total attractive interactions  $\Delta E_{elstat} + \Delta E_{orb}$ .<sup>3</sup> Values in parentheses give the percentage contribution to the orbital interactions  $\Delta E_{orb}$ .

The ligand nNHC (imidazol-2-ylidene) is a cyclic carbene with two nitrogen atoms in the  $\alpha$  positions. It is a model compound of the well-known unsaturated Arduengo-type N-heterocyclic carbenes. The tautomeric carbene aNHC (imidazol-4-ylidene) has only one nitrogen atom in  $\alpha$  position while the second nitrogen atom stabilizes the carbene center through conjugation. The third tautomer IMID is not a carbene, the  $\sigma$  lone-pair orbital resides at nitrogen.

The values in Table 6 show that the abnormal NHC has the largest interaction energy to the metal fragment (-62.1 kcal/mol), the nNHC is slightly weaker bound (-58.3 kcal/mol), while the IMID complex has by far the smallest interaction energy (-36.6 kcal/mol). The absolute values of the attractive orbital and electrostatic contributions as well as

the Pauli repulsion exhibit the same trend. Thus, electrostatic and orbital contributions overcompensate the larger Pauli repulsion in the carbene complexes compared to the IMID complex. The orbital contributions are dominated by the  $\sigma$  donation to the metal fragment. NHCs are only weak  $\pi$  acceptors, as the carbene center is already stabilized by conjugative donation of the lone pairs at nitrogen into the vacant  $\pi$  type orbital at the carbene carbon atom. Differences in the  $\sigma$  donation to metal centers correlate with the orbital energy of the  $\sigma$  donor orbital of the carbene which is higher in energy in aNHC than in nNHC. In the IMID ligand, the corresponding orbital is a lone pair at the nitrogen that is much lower in energy than the carbene lone pairs. Studies with a large number of normal and abnormal

**SCHEME 3** | (a) Schematic representation of the tautomers 'normal' N-heterocyclic carbene (nNHC), 'abnormal' N-heterocyclic carbene (aNHC) and imidazol (IMID). (b) Schematic representation of the complexes of the above ligands with  $W(CO)_5$ .

**TABLE 7** | EDA Results of Compounds  $(CO)_5W-L$  ( $L = PMe_3, PCl_3$  and  $PF_3$ ) at BP86/TZ2P

	$(CO)_5W-PMe_3$	$(CO)_5W-PF_3$	$(CO)_5W-PCl_3$
$\Delta E_{int}$	-46.4	-38.6	-31.1
$\Delta E_{Pauli}$	99.3	97.0	83.3
$\Delta E_{elstat}^1$	-94.9 (65.1%)	-70.2 (51.8%)	-55.8 (48.8%)
$\Delta E_{orb}^1$	-50.8 (34.9%)	-65.4 (48.2%)	-58.5 (51.2%)
$\Delta E(\sigma)^2$	-37.3 (73.4%)	-32.4 (49.5%)	-31.2 (53.3%)
$\Delta E(\pi)^2$	-13.5 (26.6%)	-33.1 (50.5%)	-27.3 (46.7%)
$\Delta E_{prep}$	2.6	3.1	2.5
$-D_e$	-43.8	-35.4	-28.6
$R(W-P)$	2.553	2.237	2.300

Taken from Ref 71.

Energy values in kcal/mol.

<sup>1</sup> Values in parentheses give the percentage contribution to the total attractive interactions  $\Delta E_{elstat} + \Delta E_{orb}$ .

<sup>2</sup> Values in parentheses give the percentage contribution to the orbital interactions  $\Delta E_{orb}$ .

carbenes to various transition metal centers showed that the correlation of the total interaction energies in these complexes exhibit a nearly linear correlation with the orbital energies of the  $\sigma$  donor orbitals of the ligands for each transition metal center and that  $\pi$  interactions usually play a less important role for the orbital interactions.<sup>70,76,77</sup>

Table 7 shows the EDA results of the interaction of  $(CO)_5W$  with the three phosphines  $PMe_3$ ,  $PF_3$ , and  $PCl_3$ . The results are very interesting because they demonstrate that orbital interactions do not always correlate with the trend of the bond strength!

The trimethylphosphine ligand  $PMe_3$  exhibits the largest interaction energy with the  $(CO)_5W$  fragment—but it has the smallest orbital contribution (-50.8 kcal/mol) out of all three phosphines. The  $\Delta E_{orb}$  values of the trihalophosphine ligands  $PF_3$  (-65.4 kcal/mol) and  $PCl_3$  (-58.5 kcal/mol) are significantly stronger than for  $PMe_3$ . Inspection of the  $\sigma$  and  $\pi$  contributions to  $\Delta E_{orb}$  reveals that the  $(CO)_5W \rightarrow PX_3$   $\pi$  backdonation is responsible for the stronger orbital interactions in the former complexes. This is reasonable because the trihalophosphines are better  $\pi$  acceptors than  $PMe_3$ . The Pauli repulsion exhibited by the former ligands is also larger than for the latter which leaves the electrostatic term as crucial component for the trend of the  $(CO)_5W \rightarrow PX_3$  interaction energies  $\Delta E_{int}$ . Table 7 shows that the  $\Delta E_{elstat}$  value for  $PMe_3$  (-94.9 kcal/mol) is much larger than for  $PF_3$  (-70.2 kcal/mol) and  $PCl_3$  (-55.8 kcal/mol). The latter trend can be explained with the hybridization of the  $\sigma$  lone-pair orbital at phosphorous which has a much higher percentage s

character in the trihalophosphines than in  $PMe_3$ . The higher percentage s character makes the lone-pair orbital to be more compact which yields a smaller overlap with the tungsten nucleus, which is the main component of the electrostatic attraction in  $(CO)_5W \rightarrow PX_3$ .

Inspection of the EDA results in Tables 5–7 suggests that, for most metal-ligand interactions, the electrostatic term  $\Delta E_{elstat}$  makes a larger contribution to the total metal-ligand attraction than the orbital term  $\Delta E_{orb}$ . This finding was made also for other transition metal complexes.<sup>51</sup> One wonders if the DCD bonding is really valid for explaining the nature of metal-ligand interactions. Examination of a large number of classes of transition metal complexes with different ligands show that the trend of  $\Delta E_{orb}$  is often in agreement with the trend of the total interaction energy  $\Delta E_{int}$  although the absolute values are in many cases smaller than the data for  $\Delta E_{elstat}$  and  $\Delta E_{Pauli}$ . The trend for the bond strength of the phosphine complexes shown in Table 7 is a striking example that in some cases other terms than the orbital interactions may be relevant for the trend of the bond strength. It may serve as a warning against the indiscriminate use of the orbital interactions as the sole reason for trends in bond energies.

## Bonding in the Sandwich Compounds Ferrocene and Bis(Benzene)Chromium<sup>78</sup>

The syntheses of ferrocene,  $Fe(C_5H_5)_2$ , in 1951 by Miller et al.<sup>79</sup> and Kealy and Pauson<sup>80</sup> and its structural investigation by Fischer and Pfäffle<sup>81</sup> and Woodward et al.<sup>82</sup> were landmarks of organometallic chemistry.<sup>83</sup> The explanation of the geometry, the magnetic properties and the reactivity of ferrocene in terms of bonding models was a challenging task and a matter of controversy. The correct prediction of its aromatic character by Woodward, which implied a description of a bonding of two  $Cp^-$  ligands with an  $Fe(II)$  cation as well as the synthesis of bis(benzene) chromium,  $Cr(C_6H_6)_2$ , by Fischer and Hafner,<sup>84</sup> the first example of a sandwich compound build from a metal and a ligand of formal neutral charge, were due to a successful application of bonding models.<sup>85,86</sup> Today, the ferrocene structure is well understood and can be regarded as an icon of organometallic chemistry.<sup>83</sup>

Figure 2 shows the orbital correlation diagram that illustrates the standard orbital picture of the bonding interactions of a  $d^6$  metal  $(a_{1g})^2(e_{2g})^4(e_{1g})^0$  with two  $\eta^6$  coordinated benzene rings. The

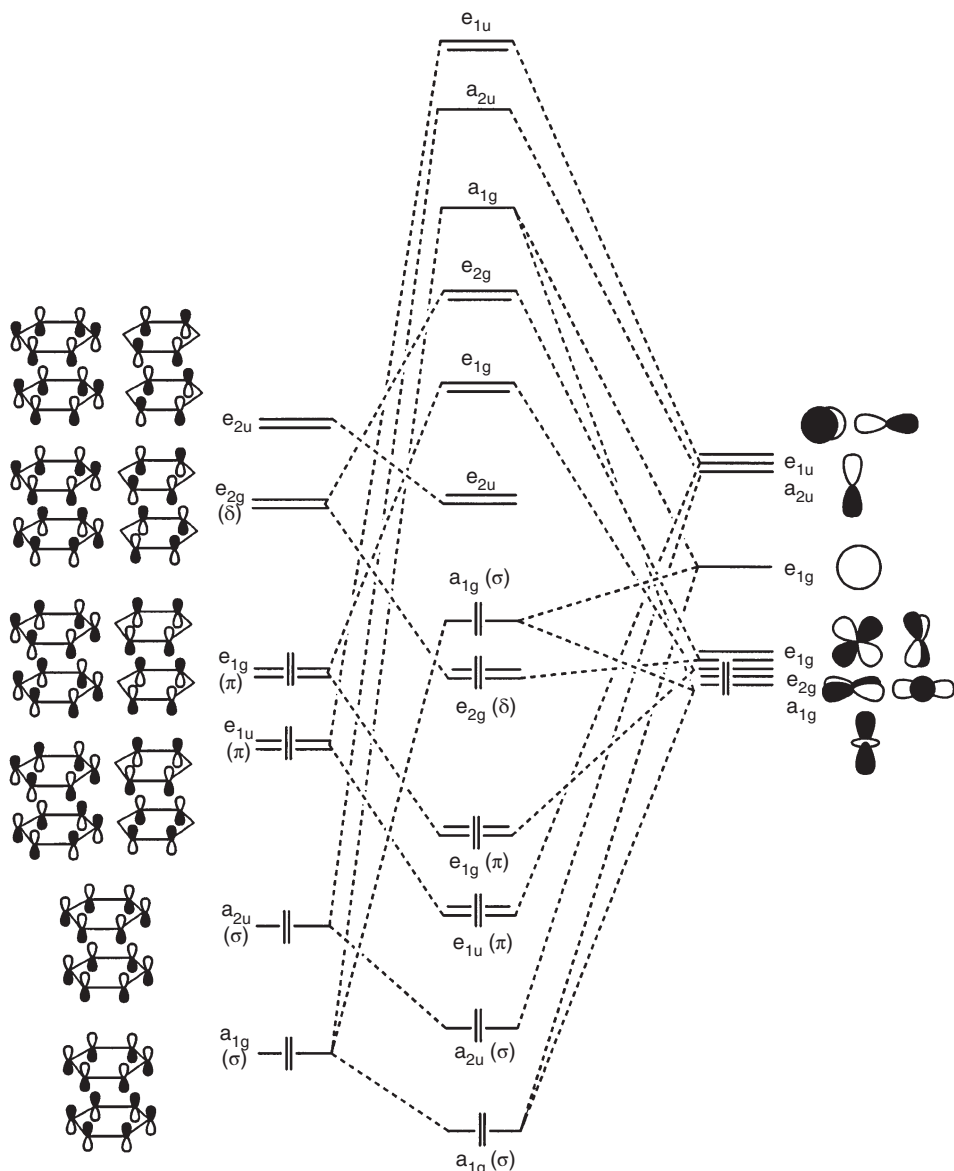


**FIGURE 2 |** MO correlation diagram between a  $d^6$  transition metal with the electronic configuration  $(a_{1g})^2(e_{2g})^6(e_{1g})^0$  and a cyclic  $12\pi$  aromatic sandwich ligand. Shapes of the orbitals have been taken from the  $Bz_2$  ligand. The orbitals of  $(Cp_2)^{2-}$  look very similar. Figure taken from Ref 78.

qualitative picture of a  $d^6$  metal with two  $Cp^-$  rings looks similar. The correlation diagram is shown for a structure which has  $D_{6h}$  symmetry where the ligands are in an eclipsed conformation which refers to the equilibrium geometry of ferrocene. A related diagram can be given for the  $D_{6d}$  structure.<sup>78</sup> Figure 2 shows that there are bonding contributions of orbitals which possess  $\sigma$ -,  $\pi$ -, and  $\delta$ -symmetry with respect to two orthogonal planes that bisect the ligand planes and that contain the main axis. Thus  $\sigma$  orbitals may have symmetries which belong to the irreducible representations  $a_{1g}$  and  $a_{2u}$ ,  $\pi$  orbitals have the

symmetries  $e_{1g}$  and  $e_{1u}$  while  $\delta$  orbitals may have  $e_{2g}$  and  $e_{2u}$ . The lowest lying nine valence orbitals of ferrocene and bis(benzene)chromium are occupied fulfilling the 18 electron rule.

Table 8 gives the results of EDA analyses of Ferrocene,  $Fe(Cp)_2$ , and bis(benzene)chromium,  $Cr(Bz)_2$  where the contributions of  $\sigma$ -,  $\pi$ -, and  $\delta$ -orbital interactions are summarized. See the original work for a detailed presentation of orbital interactions in all irreducible representations.<sup>78</sup> The breakdown of the orbital term  $\Delta E_{orb}$  into orbitals which possess different symmetry makes it possible

**TABLE 8** | Energy Decomposition Analyses of Cr(Bz)<sub>2</sub> and Fe(Cp)<sub>2</sub> at BP86/TZP.

	Cr(Bz) <sub>2</sub> Cr <sup>0</sup> [d <sub>z2</sub> , d <sub>xy</sub> , d <sub>x2-y2</sub> ] <sup>6</sup>	Fe(Cp) <sub>2</sub> Fe <sup>2+</sup> [d <sub>z2</sub> , d <sub>xy</sub> , d <sub>x2-y2</sub> ] <sup>6</sup>	Fe <sup>0</sup> [d <sub>z2</sub> , d <sub>xy</sub> , d <sub>x2-y2</sub> ] <sup>6</sup> [d <sub>xz</sub> , d <sub>yz</sub> ] <sup>6</sup>
ΔE <sub>int</sub>	-268.5	-893.9	-274.2
ΔE <sub>Pauli</sub>	339.2	279.9	409.6
ΔE <sub>elstat</sub> <sup>1</sup>	-230.5 (37.9%)	-599.9 (51.1%)	-307.5 (45.0%)
ΔE <sub>orb</sub> <sup>1</sup>	-377.2 (62.1%)	-573.9 (48.9%)	-376.3 (55.0%)
ΔE(σ) <sup>2</sup>	-38.3 (10.2%)	-76.9 (13.4%)	-27.5 (7.3%)
ΔE(π) <sup>2</sup>	-59.4 (15.7%)	-432.7 (75.4%)	-236.0 (62.7%)
ΔE(δ) <sup>2</sup>	-278.8 (73.9%)	-64.4 (11.2%)	-112.9 (30.0%)

Taken from Ref 78.

Energy values in kcal/mol.

<sup>1</sup> Values in parentheses give the percentage contribution to the total attractive interactions ΔE<sub>elstat</sub> + ΔE<sub>orb</sub>.

<sup>2</sup> Values in parentheses give the percentage contribution to the orbital interactions ΔE<sub>orb</sub>.

to quantify the strength of σ-, π-, and δ-orbital interactions in the two complexes. In the case of Cr(Bz)<sub>2</sub> the interacting fragments are the neutral chromium atom in its d<sup>6</sup> state and neutral (Bz)<sub>2</sub>. The largest attractive contribution to the total interaction energy is the orbital term (62.1%). From the decomposition of ΔE<sub>orb</sub> it becomes obvious that the orbital bonding is dominated by δ contributions (-278.8 kcal/mol, 73.9%). The σ-orbital interactions (-38.3 kcal/mol, 10.2%) and π-orbital contributions (-59.4 kcal/mol, 15.7%) are much smaller than the δ-orbital contributions.

The common bonding model for ferrocene introduces the metal–ligand interactions in terms of charged fragments Fe<sup>2+</sup> and (Cp)<sub>2</sub><sup>2-</sup>. The EDA results for the latter fragmentation scheme which are given in Table 8 show that the total interaction energy is much larger than in Cr(Bz)<sub>2</sub> (-893.9 kcal/mol vs -268.5 kcal/mol). This comes from the use of charged fragments. The orbital term still contributes 48.9% to the total attractive interactions. The energy level of the donor orbitals in (Cp)<sub>2</sub><sup>2-</sup> are much higher in energy than in neutral (Bz)<sub>2</sub> and the acceptor orbitals in Fe<sup>2+</sup> are energetically lower lying than in neutral Cr. Table 8 shows that the dominating orbital contribution in Fe(Cp)<sub>2</sub> comes from the π orbitals (-432.7 kcal/mol, 75.4%) while the σ- and δ-orbital interactions are much weaker. This result could perhaps be biased through the choice of the fragments, because the π-orbital contributions come from (Fe<sup>2+</sup>)<sup>-</sup>(Cp)<sub>2</sub><sup>2-</sup> π backdonation (Figure 3) which can be expected to be enhanced by the choice of charged moieties for the interactions in ferrocene. Table 8 shows also the EDA results where neutral fragments Fe and (Cp)<sub>2</sub> in the triplet states were chosen for the calculation. The total interaction energy is now significantly

smaller (-274.2 kcal/mol) and much closer to the value for Cr(Bz)<sub>2</sub>. Inspection of the orbital term ΔE<sub>orb</sub> shows that the π-orbital interactions still provide the largest contribution (-236.0 kcal/mol, 62.7%) to the covalent bonding. Thus, the EDA calculations suggest that ferrocene is a π bonded molecule while bis(benzene)chromium is a δ bonded complex.<sup>78</sup>

Similar studies on Ferrocene derivatives Fe( $\eta^5$ -E<sub>5</sub>)<sub>2</sub> (E = N-Sb)<sup>88,89</sup> and [Ti( $\eta^5$ -E<sub>5</sub>)<sub>2</sub>]<sup>2-</sup> (E = CH, N-Sb)<sup>90</sup> show that these compounds have isostructural energy minimum geometries and that, as in Ferrocene, the main orbital bonding contribution comes from π-orbital interactions for the iron compounds. The titanium compounds exhibit larger δ bonding.

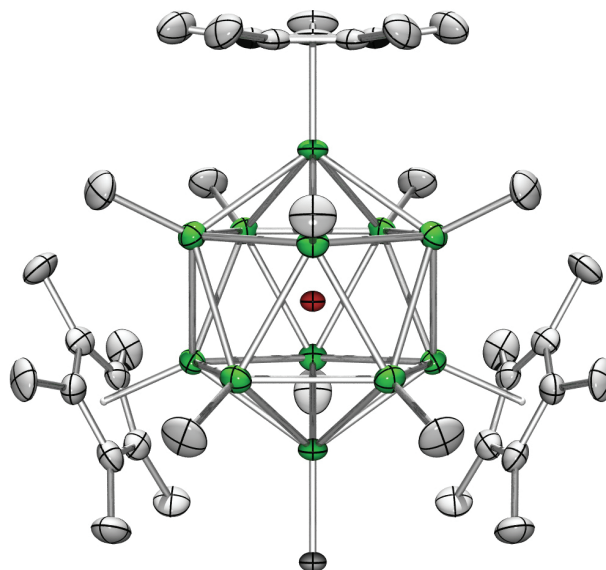


**FIGURE 3** | X-ray structure of [Mo(ZnCp\*)<sub>3</sub>](ZnMe)<sub>12</sub>. Mo red, Zn green, C gray. Figure taken from Ref 87.

Computational analyses of main group metallocenes [ $E(Cp)$ ] ( $E = Li-Cs, B-Tl$ ) and [ $E(Cp)_2$ ] ( $E = Be-Ba, Si-Pb$ ) and [ $Zn(Cp)_2$ ] show that the interaction of alkali-metal cations with  $Cp^-$  and alkaline-earth cations with  $(Cp^-)_2$  are almost exclusively electrostatic.<sup>91</sup> The lightest cations of group 1 and 2 exhibit largest relative orbital interactions to  $Cp^-$ . In most cases, the important contributions to the orbital interactions come from  $\sigma$  and  $\pi$  bonding.<sup>91</sup> Studies on multimetallocenes  $CpM_nCp$  ( $M = Be, Mg, Ca, Zn, n = 2-5$ ), inspired by the synthesis of  $Zn_2Cp^{*2}$  by Carmone et al.,<sup>92</sup> show that species with  $n > 2$  and  $M = Mg, Ca, Zn$  are thermodynamically unstable upon the loss of a metal atom. Interaction energies to the  $Cp^-$  ligands decrease with an increase of  $n$ . Largest contributions to the orbital interactions come from  $\pi$  interactions which become weaker with increasing  $n$  while the importance of the  $\sigma$  bonding increases with increasing  $n$ .<sup>93</sup>

### Bonding in the Icosahedral Compound $[Mo(ZnCp^*)_3(ZnMe)_9]$

The remarkable compound  $[Mo(ZnCp^*)_3(ZnMe)_9]$  which possesses the unusually high coordination number 12 (Figure 3) that was synthesized by R. A. Fischer et al. in 2008<sup>87</sup> poses a great challenge for bonding analysis. The central molybdenum atom is coordinated to 12 zinc atoms in an almost perfect icosahedral fashion.

At first glance the compound seems to be similar to endohedral cluster compounds like  $[Pt@Pb_{12}]^{2-}$  which was earlier synthesized by Eichhorn et al.<sup>94</sup>

**TABLE 9 |** EDA Results of  $Mo(ZnH)_{12}$ . Fragments are Mo and  $(ZnH)_{12}$  in Septet States

	$Mo(s^1d^5) + (ZnH)_{12}(a_g^1h_g^5)$
$\Delta E_{int}$	-348.8
$\Delta E_{Pauli}$	594.5
$\Delta E_{elstat}^1$	-540.1 (57.2%)
$\Delta E_{orb}^1$	-403.2 (42.8%)
$\Delta E(a_g)^2$	-96.4 (23.9%)
$\Delta E(h_g)^2$	-288.0 (71.5%)
$\Delta E(t_{1u})^2$	-18.3 (4.5%)

Taken from Ref 87.

Energy values in kcal/mol.

<sup>1</sup> Values in parentheses give the percentage contribution to the total attractive interactions  $\Delta E_{elstat} + \Delta E_{orb}$ .

<sup>2</sup> Values in parentheses give the percentage contribution to the orbital interactions  $\Delta E_{orb}$ .

The bonding of the latter species is characterized by strong peripheral interactions among the lead atoms forming a  $(Pb_{12})^{2-}$  cage while the contribution of the interactions between the central Pt atom and the  $Pb_{12}$  cage to the overall stability of the compound is much smaller. The insertion of the Pt atom into the cage only further stabilizes the cage by filling the empty center.<sup>95</sup> The stability of  $(Pb_{12})^{2-}$  cage which possesses 26 valence electrons for cluster bonding is predicted by the Wade-Mingos rules.<sup>96,97</sup> In contrast, the empty  $(ZnR)_{12}$  cage has only 12 valence electrons that are available for peripheral bonding and thus, the cage is electron deficient. In fact, computational studies showed that a geometry optimization of the empty  $(ZnR)_{12}$  cage yields decomposition into several

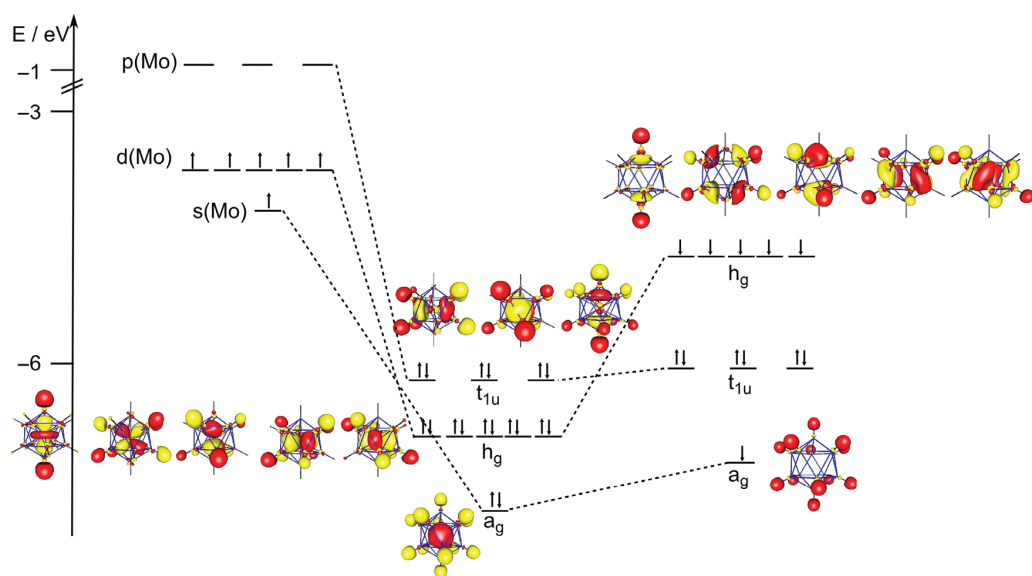


**FIGURE 4 |** MO correlation diagram between Mo and  $(ZnH)_{12}$  in  $[Mo(ZnH)_{12}]$ . Each fragment in its septet state. Figure taken from Ref 11.

fragments. Including six valence electrons of the molybdenum atom, the compound remains electron deficient in terms of the Wade-Mingos rules. Thus, a detailed analysis of the interaction of the central molybdenum atom with the 12 surrounding zinc atoms is necessary to understand the bonding in this compound. Table 9 gives the results of an EDA of the central molybdenum atom in its electronic septet ground state ( $s^1 d^5$ ) with a  $(\text{ZnH})_{12}$  moiety in the corresponding electronic state ( $a_g^1(b_g)^5$ ). A schematic correlation diagram according to this fragmentation is shown in Figure 4.

The parent compound  $[\text{Mo}(\text{ZnH})_{12}]$  was chosen as a model system for analysis as it resembles the  $\text{MoZn}_{12}$  core while it has perfect icosahedral symmetry ( $I_h$ ). Details on the choice of the model system and results of accompanying analyses of the molecular orbitals and the electron density (atoms in molecules analysis, AIM) are presented in the original article.<sup>87</sup> Figure 5 shows the highest lying occupied molecular orbitals of the parent compound. It becomes obvious, that the highest lying occupied MO (HOMO) is triply degenerated ( $t_{1g}$  irreducible representation) and that it includes only very small contributions from the molybdenum valence  $p$  orbitals. The HOMO-1 orbital is quintuply degenerated ( $b_g$ ) and exhibits orbital interactions between the  $[\text{ZnH}]_{12}$  fragment and  $d$  atomic orbitals of the Mo atom. The HOMO-2 belongs to the  $a_g$  irreducible representation showing interactions of the  $[\text{ZnH}]_{12}$  fragment with the valence  $s$  AO of Mo. The results of the EDA (Table 9) suggest that the HOMO-1 ( $b_g$ ) and HOMO-2 ( $a_g$ ) orbitals, which exhibit interactions between the  $[\text{ZnH}]_{12}$  cage and

the  $s$  and  $d$  AOs of the central atom, are much more important than orbital interactions with the  $p$  AOs of the central atom ( $t_{1g}$ ) which come from the HOMO. The latter contribute only 4.5% to  $\Delta E_{\text{orb}}$ . As the valence  $s$  and  $d$  AOs of the molybdenum atom are singly occupied, they cover the largest part of the orbital contributions through interactions with the  $[\text{ZnH}]_{12}$  fragment. Thus, a description of a  $sd^5$  hybridized central atom in terms of valence bond theory is appropriate. The six  $sd^5$  hybrid orbitals have in total 12 lobes pointing to each corner of an icosahedron (see Figure 5).<sup>99,100</sup>

The use of such a bonding model implies that each of the six singly occupied  $sd^5$  hybrid orbitals forms a 2-electron-3-center bond with two zinc atoms located at opposite corners of the icosahedron. In total, 12 valence electrons (VE) are used for these bonds. Mo provides its six valence electrons while each Zn atom contributes 1/2 electron for bonding with Mo. There remains 1/2 electron per zinc atom for orbital interactions with five identical neighboring zinc atoms resulting in only 1/10 electron pair per peripheral Zn-Zn interaction. The latter interactions are thus weak and their main role is to prevent ligand-ligand repulsion.

## FURTHER SELECTED APPLICATIONS OF THE EDA

In parts 2 and 3 of this review, we presented detailed discussions of EDA studies in order to introduce the reader to the numerical results and insights that are obtained by the method and to provide inspiration on how to connect calculated data from the EDA with chemical interpretation. The examples were chosen in order to demonstrate how to use the EDA to solve problems of chemical interest. In this last part we will summarize, without detailed discussion, some further selected studies that were performed with the EDA. In combination with the previous chapters this part demonstrates the wide applicability of the method.

### Analyzing Chemical Reactions with the Activation Strain Model

The activation strain models is an application of the EDA not on the equilibrium geometries but on transition state structures or other points along the intrinsic reaction coordinate (IRC)<sup>101</sup> of a chemical reaction. The activation energy  $\Delta E^\ddagger$  is decomposed into the strain energy  $\Delta E_{\text{strain}}^\ddagger$  that represents the distortion of two fragments from their equilibrium

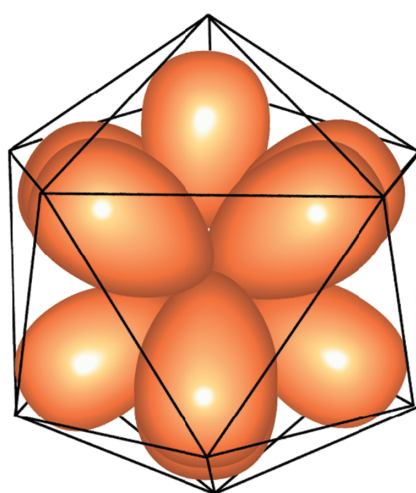


**FIGURE 5 |** Schematic representation of the six  $sd^5$  hybrid orbitals. Figure taken from Ref 87.

geometry to that in the transition state (or the investigated point on the IRC), and the interaction energy  $\Delta E_{\text{int}}^{\ddagger}$  between the two distorted fragments in the transition state. The latter can, as in the application of the EDA on ground states, be separated into Pauli, electrostatic and orbital contributions. Applications of the activation strain model include investigations of the effect of catalysts on elimination and nucleophilic substitution reactions,<sup>102–104</sup> C–X bond activation by transition metal catalysts<sup>105–112</sup> or main group metals,<sup>113</sup> oxidative addition versus dehydrogenation of EH<sub>4</sub> (E = C–Pb) in reactions with transition metals<sup>114</sup> and pericyclic reactions.<sup>115</sup> Bickelhaupt et al. summarized applications of the activation strain model in recent review articles.<sup>116–118</sup>

## Multiple Bonds in Main Group and Transition Metal Compounds

EDA were used to describe the multiple bonds between transition metals and between heavy main group elements. For example, the unusual structures of heavy-atom analogues of acetylene were explained with the help of the EDA,<sup>119</sup> enabling insight into the bonding situation of the recently synthesized compounds RPbPbR ( $R = C_6H_2-2,6-(C_6H_2-2,4,6-iPr_3)_2$ ),<sup>120</sup> REER ( $E = Ge, Sn; R = C_6H_3-2,6-(C_6H_3-2,6-iPr_2)_2$ )<sup>121,122</sup> and RSiSiR ( $R = ((CH(Me_3Si)_2)_2iPrSi)$ ).<sup>123</sup> The parent systems HEEH as well as the isolated molecules REER exhibit nonlinear equilibrium structures which show some very unusual features. HEEH structures exhibit doubly H-bridging of the E–E bond with orthogonal planes which is not possible because of steric hindrance in the synthesized molecules REER which possess bulky ligands. The unusual structures of both the parent compounds HEEH and synthesized REER could be explained in terms of fragments in the electronic doublet states. Similar effects are observed and analyzed with the EDA for heavier homologues of ethylene which exhibit trans-bent geometries.<sup>124</sup>

Early work by Ziegler<sup>125,126</sup> and more recent work by Frenking et al.<sup>127</sup> analyses the nature of multiple bonds between transition metal atoms as bond orders. Ziegler showed that in molecules M<sub>2</sub>H<sub>6</sub> (M = Cr–W) both,  $\sigma$  and  $\pi$  interactions, contribute significantly to the total orbital stabilization.<sup>125</sup> Thus, a description of the M–M bonds as triple bond is justified. In molecules M<sub>2</sub>Cl<sub>4</sub>(PH<sub>3</sub>)<sub>4</sub> (M = Mn, Tc, Re), where the M–M bonds could formally be described as quadruple bonds, it is shown that the  $\delta$ -contribution to the total orbital interaction is

negligibly small (about 0.3% of the total orbital interactions) indicating that the  $\delta$  bond is very weak. The same conclusion is found by the EDA for the dianionic system Re<sub>2</sub>Cl<sub>8</sub><sup>2-</sup> and for isoelectronic Os<sub>2</sub>Cl<sub>8</sub> by Frenking et al.<sup>127</sup> The formal triple bond in Re<sub>2</sub>Cl<sub>8</sub> is calculated to be stronger than the formal quadruple bond in Re<sub>2</sub>Cl<sub>8</sub><sup>2-</sup>.

## THE EDA–NOCV METHOD

This section of the updated paper discusses the application of the EDA–NOCV method<sup>13</sup> for the bonding analysis. The focus is on the information that is gained when the orbital term  $\Delta E_{\text{orb}}$  is divided into pairwise orbital interactions of the fragments  $\Delta E_k^{\text{orb}}$  and when the associated deformation density,  $\Delta\rho_k$  is considered. Results are presented for both, equilibrium structures and transition states.

## Carbonyl Complexes of BeO and BeCO<sub>3</sub>

Beryllium oxide has been suggested as strongest neutral Lewis acid of main group elements, which according to quantum chemical calculations binds even helium atom in HeBeO with a bond dissociation energy (BDE) of  $D_e \sim 3$  kcal/mol.<sup>128–130</sup> The carbonyl complexes OCBeO and COBeO, where CO binds through its carbon or oxygen atoms, have both been prepared in low-temperature matrices<sup>131</sup> following theoretical calculations which predict large BDEs of  $D_e = 43.3$  kcal/mol for OCBeO and  $D_e = 20.4$  kcal/mol for COBeO.<sup>132</sup> The molecules were identified by comparing the experimentally observed C–O stretching frequencies with calculated values. Theory and experiment agree that OCBeO exhibits a large C–O blue shift toward higher wave numbers by 40–50 cm<sup>-1</sup>. A blue shift of CO indicates strong OC→A  $\sigma$  donation<sup>133</sup> to a Lewis acid A in so-called nonclassical carbonyl complexes.<sup>134,135</sup> The size of the blue shift appears as experimental probe for the bond strength in such species.

There has been an ongoing search for Lewis acids that are stronger than BeO. In 2015, Zhou reported that beryllium carbonate forms stable carbonyl complexes OCBeCO<sub>3</sub> and COBeCO<sub>3</sub> and that the former adduct possesses an even higher blue shift for the C–O stretching mode of 122 cm<sup>-1</sup>.<sup>98</sup> However, calculations suggest that the BDE of OCBeCO<sub>3</sub> (28.8 kcal/mol) is significantly lower than for OCBeO. The finding of higher blue shift but weaker bond in OCBeCO<sub>3</sub> could be explained with the help of EDA–NOCV calculations.

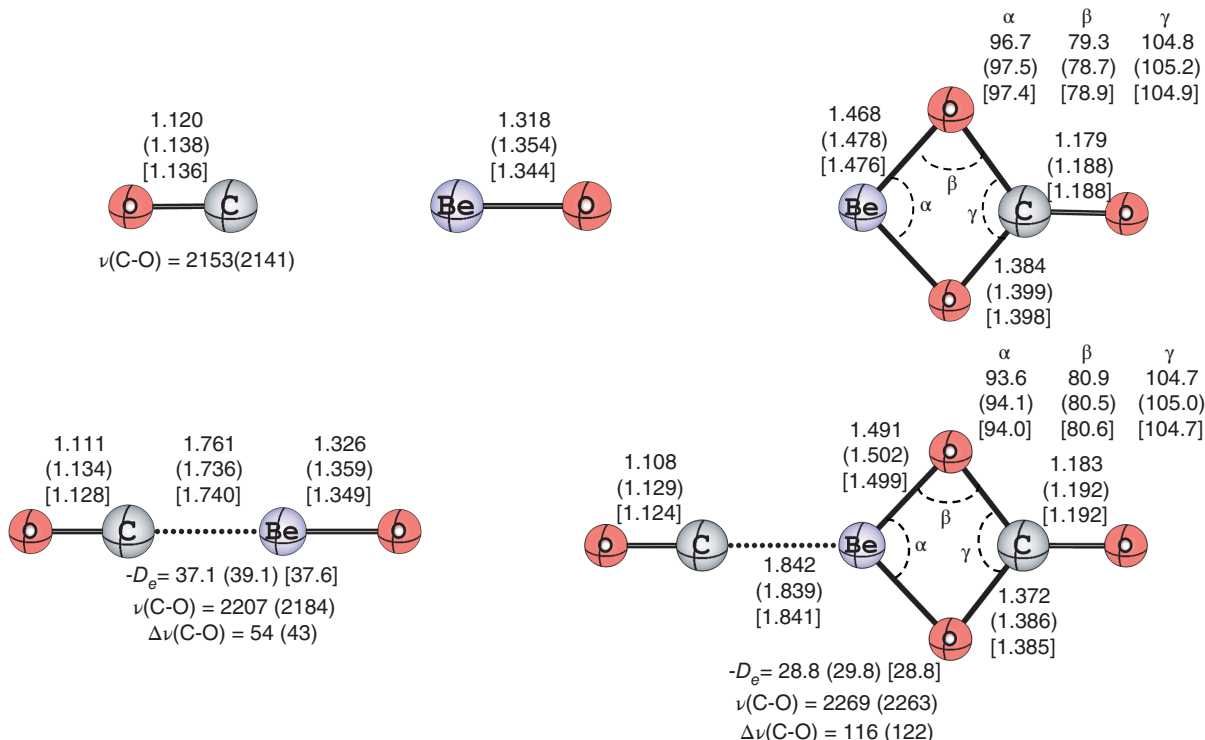


**FIGURE 6 |** Optimized geometries at M06-2X/def2-TZVPP, MP2/cc-pVTZ (in parentheses) and CCSD(T)/cc-pVTZ [in brackets]. The bond lengths and angles are in Å and °, respectively. Calculated bond dissociation energies ( $D_e$ ) for the C–Be and O–Be bond are given in kcal/mol. Theoretical CCSD(T)/cc-pVTZ (and experimental) stretching frequencies  $\nu(\text{C=O})$  and their shift  $\Delta\nu(\text{C=O})$  wrt free CO (cm<sup>-1</sup>). Figure taken from Ref 98.

Figure 6 shows the relevant results of the quantum chemical calculations of the OCBeCO<sub>3</sub> complex and the donor and acceptor fragments CO, BeO, and BeCO<sub>3</sub> at three different levels of theory, which agree quite well with each other. For a detailed discussion of the numbers we refer to the original paper.<sup>98</sup> Table 10 shows the results of the EDA–NOCV calculations. The stronger bonding of OC–BeO than in OC–BeCO<sub>3</sub> is also found in the intrinsic interactions energy  $\Delta E_{\text{int}}$  of the former species, which is 14.4 kcal/mol higher than in the latter adduct. This correlates nicely with the orbital interactions  $\Delta E_{\text{orb}}$ , which are by 15.2 kcal/mol more attractive in OC–BeO than in OC–BeCO<sub>3</sub>. Thus, the stronger carbonyl bond in OC–BeO may be explained in terms of orbital interactions.

Breakdown of the orbital term into pairwise contributions shows that the OC–BeO  $\sigma$  donation is only 2.0 kcal/mol stronger than the OC–BeCO<sub>3</sub>  $\sigma$  donation. A significantly larger difference between the two adducts is found for the  $\pi$  backdonation, which was previously not considered. The two components of the OC–BeO  $\pi$  backdonation are 11.3 kcal/mol stronger than the total OC–BeCO<sub>3</sub>  $\pi$ -backdonation. The finding of smaller blue shift but

stronger bonding in OC–BeO may thus be explained with the contribution of  $\pi$  backdonation, which along with  $\sigma$  donation enhances the bond strength but has an opposite effect on the C–O stretching mode. This finding was made possible by the

**TABLE 10 |** EDA–NOCV Results of the Chemical Bonding in OC–BeO and OC–BeCO<sub>3</sub> at BP86/TZ2P//CCSD(T)/cc-pVTZ

Fragments	OC-BeO CO and BeO	OC-BeCO <sub>3</sub> CO and BeCO <sub>3</sub>
$\Delta E_{\text{int}}$	-45.3	-30.9
$\Delta E_{\text{Pauli}}$	32.7	25.8
$\Delta E_{\text{elstat}}^1$	-31.2 (40.0%)	-25.1 (44.2%)
$\Delta E_{\text{orb}}^1$	-46.8 (60.0%)	-31.6 (55.8%)
$\Delta E_{\text{orb}}(\text{a}1)^2\sigma$	-24.5 (52.4%)	-22.5 (71.2%)
$\Delta E_{\text{orb}}(\text{b}1)^2\pi_{\parallel}$	-9.2 (19.7%)	-4.3 (13.6%)
$\Delta E_{\text{orb}}(\text{b}2)^2\pi_{\perp}$	-9.2 (19.7%)	-2.8 (8.8%)
$\Delta E_{\text{orb}}(\text{rest})^2$	-3.9 (8.3%)	-2.2 (7.0%)

Taken from Ref 98.

Energy values are given in kcal/mol.

<sup>1</sup> Values in parentheses give the percentage contribution to the total attractive interactions  $\Delta E_{\text{elstat}} + \Delta E_{\text{orb}}$ .

<sup>2</sup> Values in parentheses give the percentage contribution to the orbital interactions  $\Delta E_{\text{orb}}$ .

quantitative breakdown of the orbital term  $\Delta E_{\text{orb}}$  into its pairwise contributions.

The change in the electronic structure that comes from the pairwise orbital interactions can be visualized by the associated deformation densities  $\Delta\rho(\sigma)$  and  $\Delta\rho(\pi)$  which are connected to the  $\sigma$  donation and  $\pi$ -backdonation in OCBeO and OCBeCO<sub>3</sub>. Figure 7 graphically displays the charge flow, which is indicated by the colors red→blue. The shape of  $\Delta\rho(\sigma)$  shows that the charge flow OC→BeX (X = O, CO<sub>3</sub>) takes place in both complexes mainly from the lone-pair electrons at carbon (Figure 7(a) and (e)) to the beryllium atom. The OC→BeX  $\pi$  backdonation is coupled to an intrafragment charge transfer in CO from oxygen to carbon. It is an additional asset of the EDA–NOCV method that the bonding interactions may not only be given in terms of energy values, but the associated changes in the electronic structure can be graphically displayed.

## Electronic Structure and Bonding Situation of the Boron Dicarbonyl Complex [B(CO)<sub>2</sub>]<sup>-</sup>

The molecule carbon suboxide C<sub>3</sub>O<sub>2</sub>, which was already synthesized in 1906,<sup>136</sup> became recently the topic of renewed interest, because it was suggested that the bonding situation is better described with dative bonds OC↔C↔CO between carbon atom in the excited<sup>1</sup>D singlet state and two CO ligands rather than double bonds OC=C=CO.<sup>137</sup> The competition between  $\sigma$  donation OC→C←CO and  $\pi$

backdonation OC←C→CO using the DCD model nicely explains the finding that free carbon suboxide is not linear but has a bending angle of 156° at the central carbon atom.<sup>138–140</sup> Substitution of the central carbon atom by N<sup>+</sup> leads to a more acute bending angle of 131° in isoelectronic [N(CO)<sub>2</sub>]<sup>+</sup> because of weaker  $\pi$  backdonation OC←N<sup>+</sup>→CO.<sup>141</sup> In agreement with the bonding model, the reverse trend was observed in the boron dicarbonyl complex [B(CO)<sub>2</sub>]<sup>-</sup>, which has a linear equilibrium structure.<sup>142</sup> The question arises if the latter anion is still a donor-acceptor complex, which should be described with dative bonds OC↔B<sup>-</sup>↔O or with electron-sharing double bonds [OC=B=CO]<sup>-</sup>. This question was addressed with the help of EDA–NOCV calculations.<sup>142</sup>

The crucial information indicating the best description for the bonding situation comes from the orbital interactions, which give the energy that is associated with the bond formation. EDA–NOCV calculations were carried out with the fragments CO and B<sup>-</sup> in the electronic reference states for dative and electron-sharing bonding. These are the singlet states for dative bonding OC↔B<sup>-</sup>↔CO and quintet states for [OC=B=CO]<sup>-</sup>. Those EDA–NOCV calculations that give the smallest  $\Delta E_{\text{orb}}$  value indicate which fragments are the best choice for describing the bonding situation, because the least alteration of the electronic charge distribution is required to yield the electronic structure of the molecule. The method has been found useful in several molecules where the

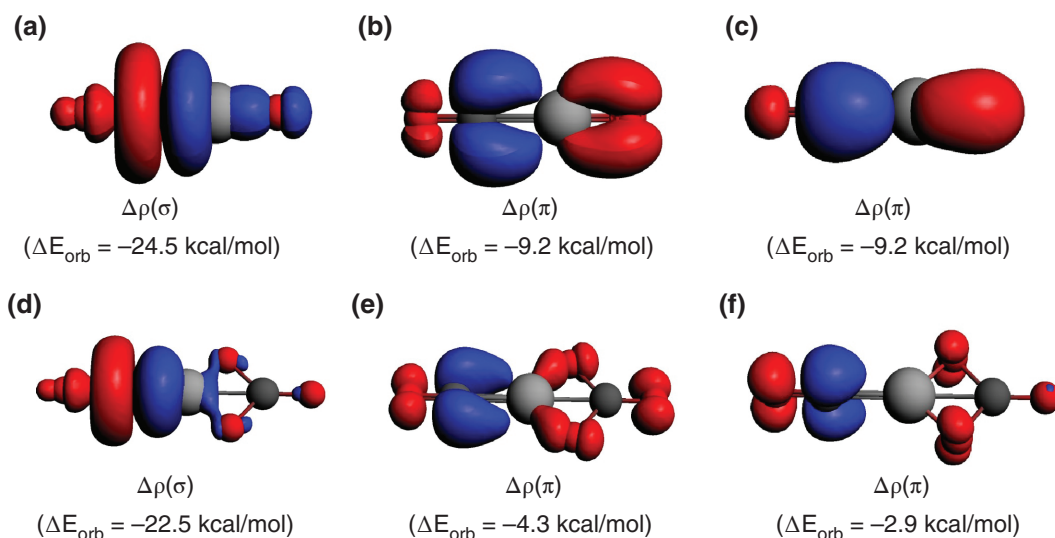


**FIGURE 7 |** Plot of deformation densities  $\Delta\rho$  of the pairwise orbital interactions and the associated interaction energies  $\Delta E_{\text{orb}}$  between CO and BeO moieties in OCBeO and OCBeCO<sub>3</sub>. The direction of the charge flow is red→blue. (a)  $\sigma$  donation OC→BeO. (b) and (c)  $\pi$  backdonation OC←BeO. (d)  $\sigma$  donation OC→BeCO<sub>3</sub>. (e) and (f)  $\pi$  backdonation OC←BeCO<sub>3</sub>. Figure taken from Ref 98.

**TABLE 11** | Energy Decomposition Analysis of  $[B(CO)_2^-]$  and  $[Al(CO)_2^-]$  at the BP86/TZ2P+ Level

Fragments	$B^- 2s^0 2p(\sigma)^0 2p(\pi)^2 2p(\pi')^2$ (OC)•••(CO) Singlet state	$B^- 2s^1 2p(\sigma)^1 2p(\pi)^1 2p(\pi')^1$ (OC)•••(CO) Quintet state
$\Delta E_{int}$	-445.3	-488.0
$\Delta E_{Pauli}$	116.7	335.0
$\Delta E_{elstat}^1$	-128.6 (22.9%)	-329.2 (40.0%)
$\Delta E_{orb}^1$	-433.4 (77.1%)	-493.9 (60.0%)
$\Delta E_1^2$ OC $\leftarrow$ E $^{(-)}\rightarrow$ CO	-127.7 (29.5%)	-87.3 (17.7%)
$\Delta E_2^2$ OC $\leftarrow$ E $^{(-)}\rightarrow$ CO	-127.7 (29.5%)	-87.3 (17.7%)
$\Delta E_3^2$ σ(+,-) OC $\rightarrow$ E $^{(-)}\leftarrow$ CO	-114.2 (26.3%)	-151.7 (30.7%)
$\Delta E_4^2$ σ(+,+) OC $\rightarrow$ E $^{(-)}\leftarrow$ CO	-54.8 (12.6%)	-151.0 (30.6%)
$\Delta E_{orb(rest)}^2$	-8.6 (2.0%)	-16.9 (3.4%)

Taken from Ref 142.

Energy values are given in kcal/mol.

<sup>1</sup> The value in parentheses gives the percentage contribution to the total attractive interactions  $\Delta E_{elstat} + \Delta E_{orb}$ .

<sup>2</sup> The value in parentheses gives the percentage contribution to the total orbital interactions  $\Delta E_{orb}$ .

nature of the bonding interactions is not obvious. The reader may find further examples in the literature.<sup>142–147</sup>

Table 11 gives the results of the EDA–NOCV calculations for  $[B(CO)_2^-]$  where the two sets of fragments were employed. It becomes obvious that the  $\Delta E_{orb}$  value for dative bonding is clearly smaller (-433.4 kcal/mol) than for electron-sharing bonding (-493.9 kcal/mol). The EDA–NOCV calculations thus suggest that the bonding situation in  $[B(CO)_2^-]$  is better described in terms of donor-acceptor interaction OC $\leftarrow$ B $^{(-)}\rightarrow$ CO. We wish to emphasize that this does not mean that the representation with classical double bonds [OC=BCO] $^-$  is wrong. Bonding models are not right or wrong, they are more or less useful. The results suggest that the description with dative bonding is a more useful account of the bond. A notable example of the usefulness to differentiate between the two types of bonding was recently reported in the literature.<sup>146</sup>

Figure 8 display the deformation densities  $\Delta\rho_1$ – $\Delta\rho_4$ , which are associated with the four largest components of  $\Delta E_{orb}$ . The shape of the deformation densities makes it easy to identify the nature of the orbital interactions, which nicely agree with the DCD model. The strongest degenerate contributions  $\Delta E_1$  and  $\Delta E_2$  (-127.7 kcal/mol each) come from the  $\pi$  backdonation OC $\leftarrow$ B $^{(-)}\rightarrow$ CO. The slightly weaker stabilization  $\Delta E_3 = -114.2$  kcal/mol arises from the out-of-phase (+,-) σ donation of the CO lone pair orbitals OC $\rightarrow$ B $^{(-)}\leftarrow$ CO into the vacant p( $\sigma$ ) AO of boron. The in-phase (+,+) σ donation OC $\rightarrow$ B $^{(-)}\leftarrow$ CO into the vacant 2 s AO of boron is much weaker ( $\Delta E_4 = -54.8$  kcal/mol) than the out-of-phase (+,-) σ donation, although the 2s AO is energetically lower

lying than the 2p AO. This is because of the larger overlap of the p( $\sigma$ ) AO than the 2s AO of boron with the donor orbitals. Figure 8 gives also the eigenvalues of the deformations densities  $|\rho_n|$  which indicate the amount of charge transfer. We want to point out that the size of  $|\rho_n|$  is not directly related to the strength of the stabilization energies  $\Delta E_n$ . A schematic representation of the dominant orbital interactions is shown at the bottom of Figure 8.

### Carbones C(PPh<sub>3</sub>)<sub>2</sub> and C(NHC<sup>Me</sup>)<sub>2</sub>

One decade ago, a previously unrecognized class of carbon compounds was discovered where two σ-donor ligands L bind to a divalent carbon(0) atom in the excited <sup>1</sup>D state *via* dative bonds L $\rightarrow$ C $\leftarrow$ L.<sup>148–150</sup> The name ‘carbone’ was coined for compound CL<sub>2</sub> where the carbon atom retains its four valence electrons as two lone pairs.<sup>151</sup> Carbones CL<sub>2</sub> differ from carbenes CR<sub>2</sub> by the number of electron lone-pairs. Carbenes are C(II) compounds with one electron lone-pair while carbones are C(0) species with two lone pairs at carbon. The parent system is carbodiphosphorane C(PPh<sub>3</sub>)<sub>2</sub>, which was synthesized already in 1961.<sup>152</sup> A detailed analysis of the electronic structure of carbodiphosphorane (CDP) revealed that the carbon-phosphorous bonds come from the donation of the phosphine groups to the carbon atom.<sup>148–150</sup> The application of the bonding model to carbon suboxide, which is mentioned in the previous section, provided a straightforward explanation for its nonlinear equilibrium structure.<sup>153,154</sup>

The bonding analysis of CDP led to the prediction that a similar structure should be found in carbodicarbene C(NHC)<sub>2</sub> where the phosphine ligands are replaced by NHC species.<sup>155,156</sup> Experimental

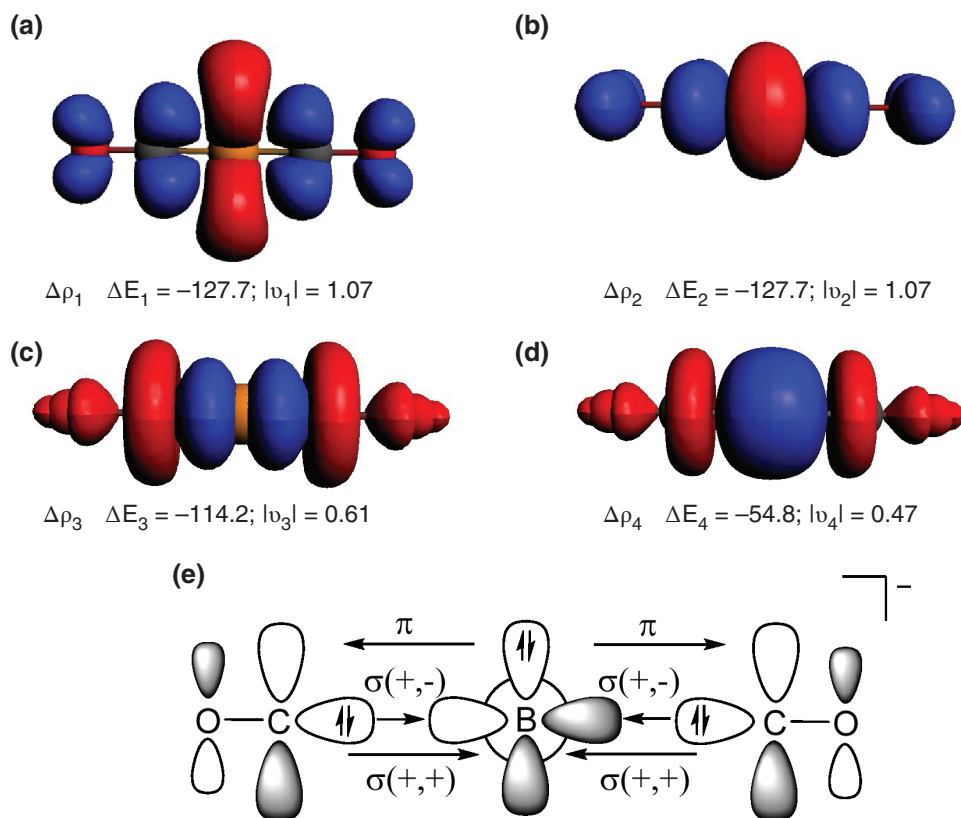


**FIGURE 8 |** (a)–(d). Plot of deformation densities  $\Delta\rho_1$ – $\Delta\rho_4$  (isocontour 0.003 a.u.) of the pairwise orbital interactions in  $[B(CO)_2]^-$  together with the associated interaction energies  $\Delta E_n$  and charge eigenvalues  $|\nu_n|$  (in e). The charge flow is red→blue. The charge eigenvalues  $\nu$  give the amount of donated/accepted electronic charge. (e) Schematic representation of the orbitals involved in the  $OC \rightarrow B^{(-)} \leftarrow CO$   $\sigma$  donation and the  $OC \leftarrow B^{(-)} \rightarrow CO$   $\pi$ -backdonation. Only one component of the latter is shown. Figure taken from Ref 142.

studies of transition metal complexes suggested that  $PR_3$  and NHC ligands exhibit similar properties as ligands.<sup>157</sup> Calculations showed in 2007 that  $C(PPh_3)_2$  and  $C(NHC^{Me})_2$  have similar bending angles of  $\sim 135^\circ$  at the central carbon atom.<sup>155,156</sup> This was confirmed in 2008 by the first syntheses of carbodicarbenes  $C(NHC^R)_2$  which possess strongly bent geometries.<sup>158–160</sup>

A schematic presentation of the bonding in carbenes  $CL_2$  is shown in Figure 9(a). Figure 9(b) displays the relevant orbital interactions  $L \rightarrow C \leftarrow L$  in more detail. There is  $\sigma$  donation from the ligand lone-pair electrons *via* the in-phase combination  $\sigma(+,+)$  into the vacant  $2p_\sigma$  AO of carbon and through out-of-phase  $\sigma(+,-)$  combination into the  $2p_{\pi\parallel}$  AO of C. The  $\pi$  electron lone-pair of carbon may engage to some degree in  $\pi$  backdonation to the ligands  $L \leftarrow C \rightarrow L$  whose size depends on the acceptor strength of L. It is shown in the previous section that the  $\pi$  backdonation in  $[B(CO)_2]^-$  may become stronger than the  $\sigma$  donation, because  $B^-$  is a strong donor and CO is a rather strong  $\pi$ -acceptor. How is the

situation in  $C(PPh_3)_2$  and  $C(NHC^{Me})_2$ ? Are the ligand properties (donation and backdonation) really similar? This question can be addressed with EDA-NOCV calculations.

Table 12 gives the numerical results of the EDA-NOCV calculations of  $C(PPh_3)_2$  and  $C(NHC^{Me})_2$ .<sup>161</sup> The NHC<sup>Me</sup> ligand is more strongly

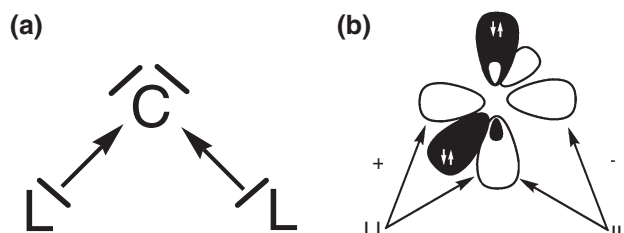


**FIGURE 9 |** Sketch of the bonding situation in carbenes  $CL_2$ . (a) Lewis structure. (b) Donation of the lone pair electrons of L into vacant orbitals of carbon. The in-phase (+,+) combination of the lone-pair electrons donates charge into the sp-hybridized  $\sigma$ -AO of C while the out-of-phase (+,-) combination of the lone-pairs donates charge into the  $2p_{\pi\parallel}$  AO of carbon.

**TABLE 12** | EDA-NOCV Calculations at the BP86/TZ2P+ Level of the Carbones  $\text{CL}_2$  Where  $\text{L} = (\text{PPh}_3)_2$ ,  $(\text{NHC}^{\text{Me}})_2$  Using the Fragments  $\text{C}$  ( $2s^2 2p_x^0 2p_y^0 2p_z^2$ ) and  $\text{L}_2$  in the Electronic Singlet States

	$\text{L} = \text{PPh}_3$	$\text{L} = \text{NHC}$
$\Delta E_{\text{int}}$	-192.0	-267.7
$\Delta E_{\text{Pauli}}$	740.8	919.1
$\Delta E_{\text{elstat}}^1$	-283.9 (30.4%)	-353.8 (29.8%)
$\Delta E_{\text{orb}}^1$	-648.9 (69.6%)	-833.1 (70.2%)
$\Delta E_1^2 \sigma(+,+)$ ( $\text{L} \rightarrow \text{C} \leftarrow \text{L}$ )	-360.8 (55.6%)	-482.0 (57.9%)
$\Delta E_2^2 \sigma(+,-)$ ( $\text{L} \rightarrow \text{C} \leftarrow \text{L}$ )	-194.6 (30.0%)	-198.6 (23.8%)
$\Delta E_3^2 \pi$ ( $\text{L} \leftarrow \text{C} \rightarrow \text{L}$ )	-59.3 (9.1%)	-97.3 (11.7%)
$\Delta E_{\text{orb}}(\text{rest})^2$	-34.2 (5.3%)	-55.2 (6.6%)

Data are taken from Ref 161.

Energy values are given in kcal/mol.

<sup>1</sup> The value in parentheses gives the percentage contribution to the total attractive interactions  $\Delta E_{\text{elstat}} + \Delta E_{\text{orb}}$ .

<sup>2</sup> The value in parentheses gives the percentage contribution to the total orbital interactions  $\Delta E_{\text{orb}}$ .

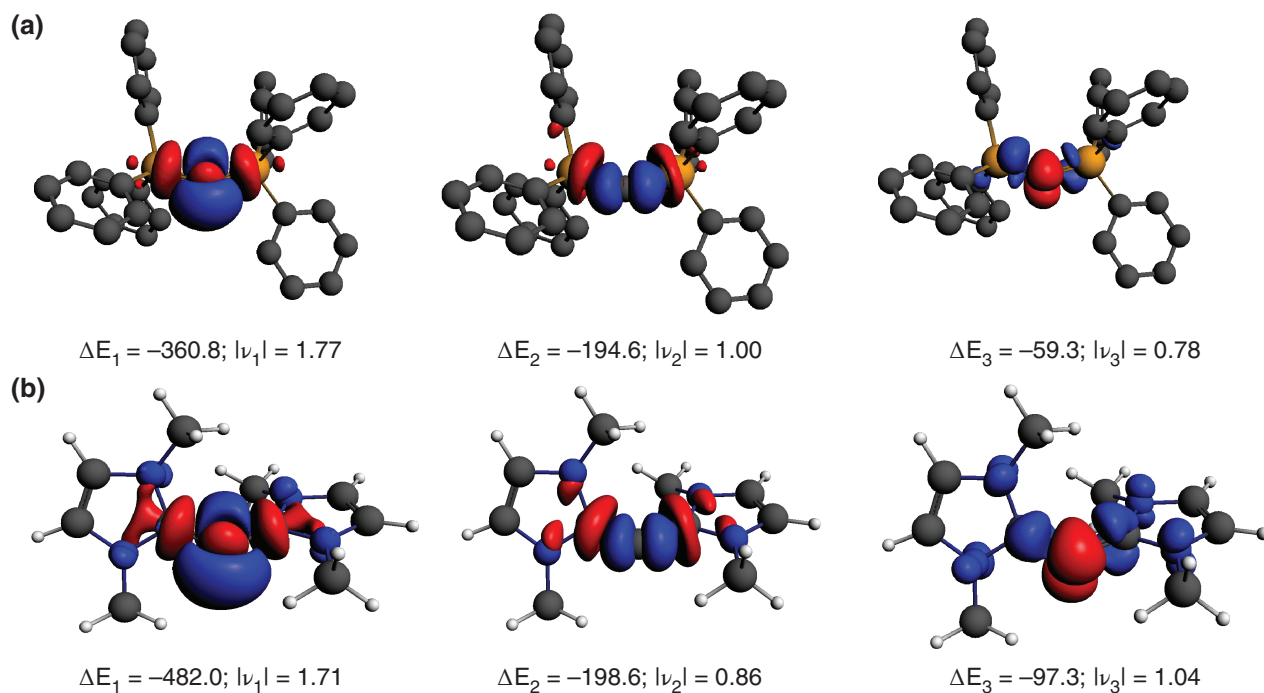
bonded ( $\Delta E_{\text{int}} = -267.7$  kcal/mol) than  $\text{PPh}_3$  ( $\Delta E_{\text{int}} = -192.0$  kcal/mol). This is reasonable, because carbenes are stronger donors than phosphines. The most important results come from the breakdown of the interaction energy into its components and from the comparison of the various orbital contributions to  $\Delta E_{\text{orb}}$ . The data suggest that the ratio of electrostatic attraction  $\Delta E_{\text{elstat}}$  to covalent bonding  $\Delta E_{\text{orb}}$  is for both system ~30:70. The strongest contribution to the orbital term  $\Delta E_{\text{orb}}$  come from the in-phase (+,+)  $\sigma$  donation  $\text{L} \rightarrow \text{C} \leftarrow \text{L}$  (56–58%) followed by the out-of-phase (+,-)  $\sigma$  donation (24% and 30%). The  $\pi$ -backdonation  $\text{L} \leftarrow \text{C} \rightarrow \text{L}$  provides in both complexes only 10–12% of the orbital interactions. The EDA-NOCV calculations support quantitatively the suggestion that phosphine and NHC ligand have very similar bonding properties.

Figure 10 displays the deformation densities are associated with the dominant orbital interaction energies  $\Delta E_{1-3}$  in the two carbenes. The shape of  $\Delta\rho_{1-3}$  exhibit the expected direction of the charge migration. A closer examination of  $\Delta\rho_1$ , which is associated with the  $\sigma(+,+)$  donation  $\text{L} \rightarrow \text{C} \leftarrow \text{L}$  indicates that there are blue regions of charge accumulation but also red regions of charge depletion at the carbon atom, which signals strong hybridization between the 2s and the  $2p_{\sigma}$  AOs. That is because the EDA-NOCV calculation starts with pure atomic orbitals for the naked carbon atom. The  $\text{L} \leftarrow \text{C} \rightarrow \text{L}$   $\pi$  backdonation in  $\text{C}(\text{PPh}_3)_2$  accumulates charge mainly at the phosphorous atom while the accrued electronic charge at the  $\text{NHC}^{\text{Me}}$  ligands is distributed to carbon and the nitrogen atoms. Note that the order of the charge eigenvalues  $v_n$  does not always agree with the order of the associated energy values  $\Delta E_n$ .

### Boron–Boron Triple Bond in $\text{B}_2(\text{NHC}^{\text{R}})_2$

In 2011, a theoretical study was published, which reported (vida infra) the calculated equilibrium geometries of the group-13 complexes  $\text{E}_2(\text{NHC}^{\text{Me}})_2$  where  $\text{E} = \text{B} - \text{In}$ .<sup>162</sup> All structures had a trans-bent geometry except for the boron system, which exhibited a linear form with a very short B-B distance. The calculated value of 1.470 Å is in accord with a standard value for a  $\text{B} \equiv \text{B}$  triple bond (1.46 Å).<sup>163</sup> The bonding situation was explained in terms of dative bonds between  $\text{B}_2$  in the highly excited (3)  ${}^1\Sigma_g^+$  state and the carbene ligands where the  $(\text{NHC}^{\text{Me}}) \rightarrow \text{B}_2 \leftarrow (\text{NHC}^{\text{Me}})$   $\sigma$  donation is supported by significant  $(\text{NHC}^{\text{Me}}) \leftarrow \text{B} \equiv \text{B} \rightarrow (\text{NHC}^{\text{Me}})$   $\pi$  backdonation. One year later, the complex  $\text{B}_2(\text{NHC}^{\text{Dip}})_2$  was synthesized and structurally characterized by Braunschweig and co-workers.<sup>164,165</sup> The X-ray structure analysis gave a B-B distance of 1.449 Å, which closely matches the calculated value. It was the first compound with a boron–boron triple bond that could be isolated and structurally characterized.<sup>166,167</sup> The related dicarbonyl complex  $\text{B}_2(\text{CO})_2$ , which was reported in 2002 by Zhou et al., is only stable in a low-temperature matrix.<sup>168</sup> Theoretical studies suggested that  $\text{B}_2(\text{CO})_2$  has a very short B–B bond of ~1.46 Å that agrees with a triple bond in the complex  $\text{OC} \rightarrow (\text{B}_2) \leftarrow \text{CO}$ .<sup>169,170</sup>

The assignment of a triple bond in  $\text{B}_2(\text{NHC}^{\text{Dip}})_2$  was challenged, and on the basis of comparing experimental data from known boron compounds with the results for  $\text{B}_2(\text{NHC}^{\text{Dip}})_2$  it was suggested that there is only a bond order of 1.5 for the boron–boron bond.<sup>171</sup> Examination of the latter study showed that the arguments are faulty and that the molecule has clearly a  $\text{B} \equiv \text{B}$  triple bond.<sup>172–174</sup> EDA–NOCV calculations of  $\text{B}_2(\text{NHC}^{\text{Me}})_2$  gave a



**FIGURE 10** | Plot of the deformation densities  $\Delta\rho$  of the most important orbital interactions in (a)  $C(PPh_3)_2$  and (b)  $C(NHC^{Me})_2$  between C in the excited  $^1D$  electronic reference state and the ligands  $L_2$  in the frozen geometry of the molecule. Associated stabilization energies  $\Delta E_1 - \Delta E_3$  are given in kcal/mol (see also Table 12). The eigenvalues  $|\nu_1| - |\nu_3|$  indicate the size of the charge deformation. The color code of the charge flow is red→blue. Figure taken from Ref 161.

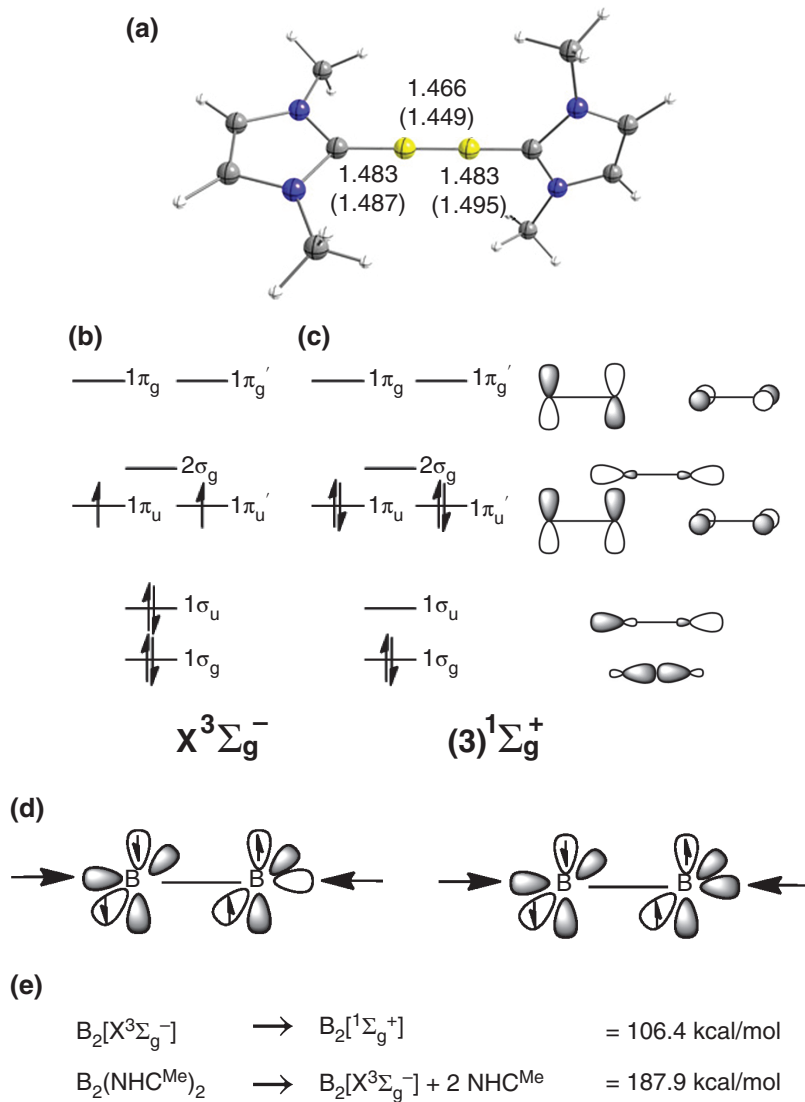
detailed insight into the nature of the bonding. The topic is a nice example for connecting the experimental geometry with a qualitative bonding model and a quantitative charge- and energy partitioning analysis of the electronic structure. The procedure demonstrates the power of modern methods of bonding analyses, which should be employed in the present time.

Figure 11 shows the equilibrium geometry of  $B_2(NHC^{Me})_2$  and the MO diagram of  $B_2$  in the  $X^3\Sigma_g^-$  ground state and the  $(3)^1\Sigma_g^+$  excited state. The latter state is the reference state of  $B_2$  in the complex, because it possesses two vacant  $\sigma$  orbitals ( $1\sigma_u$  and  $2\sigma_g$ ) that are available as acceptor orbitals for  $\sigma$  donation from the ligands  $(NHC^{Me}) \rightarrow B_2 \leftarrow (NHC^{Me})$ . This is shown in Figure 11(d). There are also two doubly occupied  $\pi$  MOs ( $1\pi_u$  and  $1\pi_u'$ ), which can engage in  $(NHC^{Me}) \leftarrow B \equiv B \rightarrow (NHC^{Me})$   $\pi$ -backdonation. The calculated excitation energy  $X^3\Sigma_g^- \rightarrow (3)^1\Sigma_g^+$  is rather high (106.4 kcal/mol), but it is clearly compensated by the strength of the donor-acceptor interactions. The calculated BDE of  $B_2(NHC^{Me})_2$  for the loss of the  $NHC^{Me}$  yielding  $B_2$  in the  $X^3\Sigma_g^-$  ground state is  $D_e = 187.9$  kcal/mol.<sup>172</sup> This means that the intrinsic binding energy between the ligands and  $B_2$  in the  $(3)^1\Sigma_g^+$  excited state is in the order of 294 kcal/mol. There is not only a strong

$B \equiv B$  triple bond in  $B_2(NHC^{Me})_2$ , but also the  $B-(NHC^{Me})$  bonds are very strong.

Table 13 shows the numerical results of the EDA-NOCV calculations of  $B_2(L)_2$  ( $L = NHC^{Me}$ , CO) where the fragments  $B_2$  and L are taken in the singlet states for dative bonding  $L \leftrightharpoons B_2 \leftrightharpoons L$  and the triplet states for electron-sharing bonding  $L = B_2 = L$ .<sup>175</sup> It becomes obvious that the former description is better suited for the bonding situation than the latter. The  $\Delta E_{orb}$  values for the interactions between the singlet states are in both cases significantly smaller than for the triplet states. The orbital interactions come from four major contributions that can easily be identified with the help of the associated deformations densities. The two  $\pi$  orbital interactions in  $B_2(CO)_2$  are degenerate, because of the  $D_{\infty h}$  symmetry of the molecule. The dihedral angle between the  $NHC^{Me}$  planes in  $B_2(NHC^{Me})_2$  deviates from  $90^\circ$  and therefore, the  $\pi$  bonding contributions in the complex have different values.

Figure 12 shows the plots of the deformation densities  $\Delta\rho_{1-4}$  together with the associated MOs of  $B_2(NHC^{Me})_2$  and the interacting fragments  $B_2$  and  $(NHC^{Me})_2$ . It becomes obvious that the  $(+,+)$   $\sigma$  donation  $NHC^{Me} \rightarrow B_2 \leftarrow NHC^{Me}$  from the HOMO-1 of  $(NHC^{Me})_2$  into the LUMO + 1 of  $B_2$  [ $(3)^1\Sigma_g^+$ ] yields a charge flow into the B-C and B-B bonding region



**FIGURE 11 |** (a) Calculated geometry at BP86/TZVPP of the complex  $\text{B}_2(\text{NHC}^{\text{Me}})_2$  with the most important bond lengths in Å. Experimental values of the analogous complex  $\text{B}_2(\text{NHC}^{\text{DIP}})_2$  are shown in parentheses. Schematic MO diagram of  $\text{B}_2$  in (b) the  $\text{X}^3\Sigma_g^-$  ground state; (c)  $(3)^1\Sigma_g^+$  excited state. (d) Schematic view of out-of-phase (+,-) and in-phase (+,+)  $\sigma$  donation of the ligand orbitals into the vacant  $1\sigma_u$  und  $2\sigma_g$  MOs of  $\text{B}_2$ . (e) Calculated excitation energy  $\Delta E$  for  $\text{X}^3\Sigma_g^- \rightarrow (3)^1\Sigma_g^+$  of  $\text{B}_2$  and bond dissociation energy  $D_e$  of  $\text{B}_2(\text{NHC}^{\text{Me}})_2$ . Figure taken from Ref 172.

(Figure 12(a)). The weaker (+,-)  $\sigma$  donation from the HOMO of  $(\text{NHC}^{\text{Me}})_2$  into the LUMO of  $\text{B}_2$  [ $(3)^1\Sigma_g^+$ ] strengthens the B-C but weakens the B–B bond region (Figure 12(b)). The two components of the  $\text{NHC}^{\text{Me}} \leftarrow \text{B}_2 \rightarrow \text{NHC}^{\text{Me}}$   $\pi$  backdonation are due to the charge flow from the degenerate HOMO of  $\text{B}_2$  [ $(3)^1\Sigma_g^+$ ] into the LUMO + 2 and LUMO + 3 of  $(\text{NHC}^{\text{Me}})_2$ . The significant contribution of the  $\text{NHC}^{\text{Me}} \leftarrow \text{B}_2 \rightarrow \text{NHC}^{\text{Me}}$   $\pi$  backdonation explains why the calculated force constant of  $\text{B}_2(\text{NHC}^{\text{Me}})_2$  gives an effective bond order of only 2.34.<sup>172</sup> The B-B  $\sigma$  bonding of HOMO-6 may formally be considered as being canceled by the B-B  $\sigma$  antibonding contribution of HOMO-13 (Figure 12(a) and (b)). The overall B-B

$\sigma$ -bond comes from the lower lying  $1\sigma_g$  MO of  $\text{B}_2$  (Figure 11). It is not relevant for the interactions between  $\text{B}_2$  and  $(\text{NHC}^{\text{Me}})_2$  and therefore it is not shown in Figure 12. Occupation of the vacant  $1\sigma_u$  and  $2\sigma_g$  MOs of  $\text{B}_2$  in the  $(3)^1\Sigma_g^+$  state gives an orbital scheme that is akin to  $\text{N}_2$  in the  $\text{X}^1\Sigma_g^+$  electronic ground state, which clearly has a triple bond.

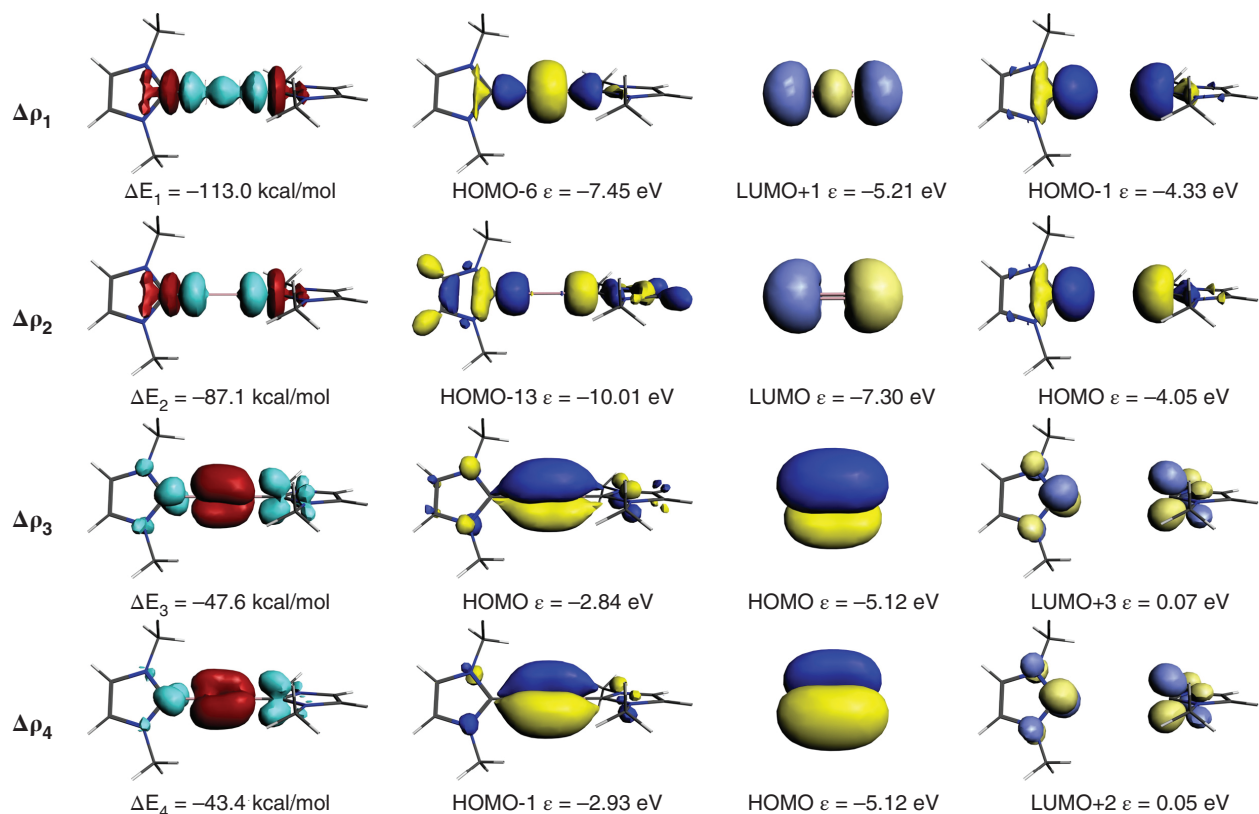
### Transition States for Addition of $\text{H}_2$ to an Amidodigermyne

The frontier MO (FMO) theory that was developed by Fukui suggests that the dominant orbital interactions between the interacting species come from the

**TABLE 13** | EDA–NOCV Results at the BP86+D3(BJ)/TZ2P+ level of Theory of Diboron Complexes  $B_2L_2$  Using Different Electronic States of the Singlet (S) and Triplet (T) Fragments

$B_2L_2$ Fragments Bonding	$B_2(NHC^{Me})_2$		$B_2(CO)_2$	
	$B_2$ (S) + $(NHC^{Me})_2$ (S) Dative	$B_2$ (T) + $(NHC^{Me})_2$ (T) Electron-sharing	$B_2$ (S) + $(CO)_2$ (S) Dative	$B_2$ (T) + $(CO)_2$ (T) Electron-sharing
$\Delta E_{int}$	-317.0	-304.8	-270.7	-483.3
$\Delta E_{Pauli}$	259.7	628.3	202.1	247.6
$\Delta E_{disp}$	-9.1	-9.1	-2.7	-2.7
$\Delta E_{elstat}^1$	-252.5 (44.5%)	-359.8 (38.9%)	-118.8 (25.3%)	-212.7 (29.2%)
$\Delta E_{orb}^1$	-315.2 (55.5%)	-564.3 (61.1%)	-351.4 (74.7%)	-515.6 (70.8%)
$\Delta E_1^2 \sigma (+,+)$ ( $L \rightarrow (B_2) \leftarrow L$ )	-113.0 (35.9%)		-100.8 (28.7%)	
$\Delta E_2^2 \sigma (+,-)$ ( $L \rightarrow (B_2) \leftarrow L$ )	-87.1 (27.6%)		-86.2 (24.5%)	
$\Delta E_3^2 \pi (L \leftarrow (B_2) \rightarrow L)$	-47.6 (15.1%)		-71.2 (20.3%)	
$\Delta E_4^2 \pi (L \leftarrow (B_2) \rightarrow L)$	-43.4 (13.8%)		-71.2 (20.3%)	
$\Delta E_{orb}(\text{rest})^2$	-24.1 (7.6%)		-22.0 (6.3%)	

Energy values are given in kcal/mol.

<sup>1</sup> The values in parentheses give the percentage contribution to the total attractive interactions  $\Delta E_{elstat} + \Delta E_{orb}$ .<sup>2</sup> The values in parentheses give the percentage contribution to the total orbital interactions  $\Delta E_{orb}$ .**FIGURE 12** | First column: Plot of the deformation densities  $\Delta\rho_{1-4}$  with associated stabilization energies  $\Delta E_{1-4}$  of the four most important orbital interactions in  $B_2(NHC^{Me})_2$ . The color code for the charge flow is red→light blue. Third and fourth column: Plot of the interacting donor and acceptor orbitals and calculated eigenvalues  $\varepsilon$  of  $(NHC^{Me})_2$  and  $(^1\Sigma_g^+)$   $B_2$ . Second column: Resulting MOs of the complex  $B_2(NHC^{Me})_2$ . Figure taken from Ref 172.

energetically highest lying occupied MO (HOMO) and the energetically lowest lying unoccupied MO (LUMO).<sup>14</sup> The FMO theory has become one of the most important chemical models for explaining chemical reactivity,<sup>176</sup> along with the orbital symmetry rules suggested by Woodward and Hoffmann (WH).<sup>15</sup> This is somewhat surprising, because the FMO theory and WH rules consider the orbitals of the separated fragments in their equilibrium geometries, but the interacting species are often significantly deformed in the transition state for a reaction. How are the fragment orbitals at the transition state connected to the orbitals of the free species? This question can be addressed with the help of EDA–NOCV calculations of the transition state. The first study where the EDA–NOCV method was employed for analyzing the orbital interactions at the transition state was recently reported by Hermann, Jones and Frenking, who investigated the reaction mechanism for H<sub>2</sub> addition to amidodigermynes (R<sub>2</sub>N)GeGe(NR<sub>2</sub>).<sup>177</sup> Details about the reaction profile can be found in their work. Here we present the analysis of the orbital interactions at the transition state for the

first step of the reaction for H<sub>2</sub> + (Me<sub>2</sub>N)GeGe(NMe<sub>2</sub>) (**1Ge**).

Figure 13 shows the calculated geometry of the transition state, where H<sub>2</sub> approaches one of the germanium atom of **1Ge**, which has a vacant  $\pi(\text{Ge}_2)$  MO and  $\sigma$  lone-pair orbitals at the Ge atoms. Qualitative FMO arguments suggest that the most important orbital interactions should come from the HOMO(H<sub>2</sub>)→LUMO(**1Ge**) donation and the reverse backdonation LUMO(H<sub>2</sub>)←HOMO(**1Ge**). The shape of the four frontier orbitals, which were calculated from the isolated species using the frozen geometries at the transition states are also shown in Figure 13. The EDA–NOCV calculations gave two major components  $\Delta E_1$  and  $\Delta E_2$  for the orbital interactions  $\Delta E_{\text{orb}}$ , which have nearly the same strength.<sup>177</sup> The (H<sub>2</sub>)→(**1Ge**) donation is slightly stronger (-37.0 kcal/mol) than the backdonation (H<sub>2</sub>)←(**1Ge**) (-35.1 kcal/mol). But the shape of the associated deformation densities  $\Delta\rho(1)$  and  $\Delta\rho(2)$  indicate that the interacting orbitals of the fragments are not only the HOMO and LUMO. Further inspection of the EDA–NOCV results reveals

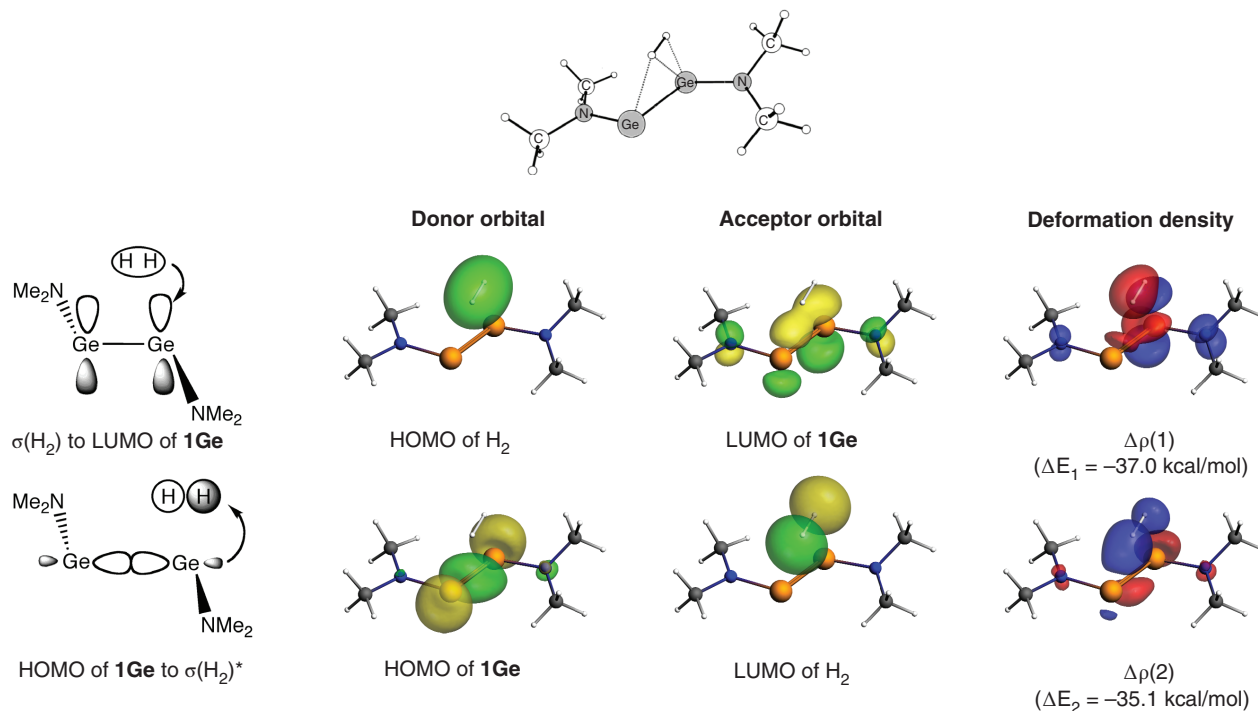


**FIGURE 13 |** Top: Calculated transition state for H<sub>2</sub> addition to the amido digermyne **1Ge**. Middle row: Schematic representation of the orbital interaction between the  $\sigma(\text{H}_2)$  MO and the LUMO of **1Ge**. Shape of the HOMO of H<sub>2</sub> and LUMO of **1Ge**. Plot of the deformation density  $\Delta\rho(1)$  which is associated with the strongest orbital interaction  $\Delta E_1$  between H<sub>2</sub> and **1Ge** in the transition state. Bottom row: Schematic representation of the orbital interaction between the HOMO of **1Ge** and the  $\sigma(\text{H}_2)^*$  MO of H<sub>2</sub>. Shape of the HOMO of **1Ge** and LUMO of H<sub>2</sub>. Plot of the deformation density  $\Delta\rho(2)$  which is associated with the second strongest orbital interaction  $\Delta E_2$  between H<sub>2</sub> and **1Ge** in the transition state. The color code for the charge flow is red→blue. Figure taken from Ref 177.

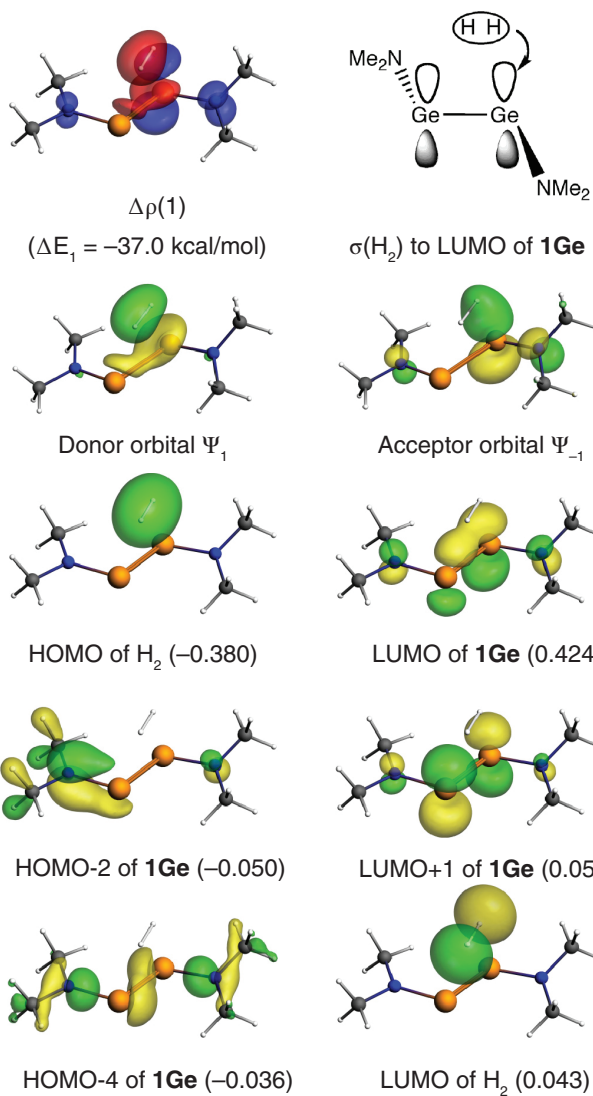


**FIGURE 14 |** Breakdown of the actual donor orbital  $\Psi_1$  and acceptor orbital  $\Psi_{-1}$  that are associated with the deformation density  $\Delta\rho(1)$  in the transition state for  $H_2$  addition to the amido digermyne **1Ge** into the most important MOs of the fragments. The mixing coefficients that are given in parentheses show that the donor orbital  $\Psi_1$  is mainly composed of the HOMO of  $H_2$  and the acceptor orbital  $\Psi_{-1}$  is mainly composed of the LUMO of **1Ge**. The contributions of further four MOs of the fragments are much smaller.

that the  $(H_2)\rightarrow(1Ge)$  donation comes from a mixture of three occupied MOs of the fragments that are the most important components of the donor MO and three vacant MOs which yield the acceptor MO. The shape of the most important fragment MOs of  $H_2$  and **1Ge** are shown in Figure 14.

Inspection of Figure 14 reveals that the donor and acceptor orbitals  $\Psi_1$  and  $\Psi_{-1}$  of the transition state, which describe the  $(H_2)\rightarrow(1Ge)$  donation are indeed mainly composed of the HOMO of  $H_2$  and

the LUMO of **1Ge**. The absolute values of the mixing coefficients of the latter frontier orbitals are much larger (0.380 and 0.424) than the coefficients of the further four orbitals that are shown in Figure 14 (0.043–0.057). They serve as polarizing contributions to the genuine FMOs for optimal interactions. The calculated numbers are a remarkable support of the original FMO theory.

A similar finding comes from the inspection of the orbital contributions to the donor and acceptor orbitals  $\Psi_2$  and  $\Psi_{-2}$  of the transition state, which describe the backdonation  $(H_2)\leftarrow(1Ge)$ . They are shown in Figure 15. The HOMO of **1Ge** and the

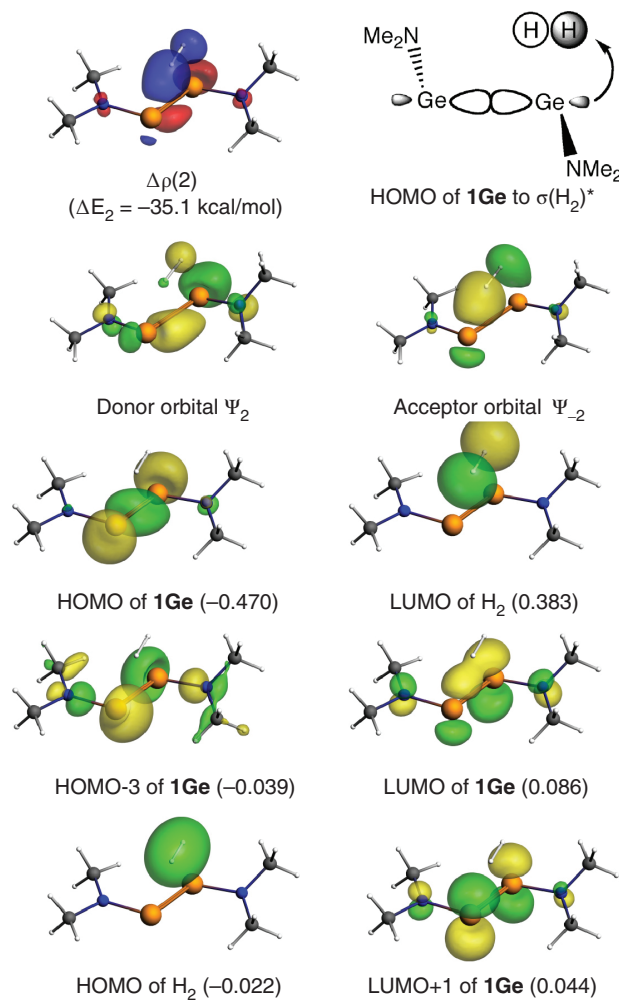


**FIGURE 15 |** Breakdown of the actual donor orbital  $\Psi_2$  and acceptor orbital  $\Psi_{-2}$  that are associated with the deformation density  $\Delta\rho(2)$  in the transition state for  $H_2$  addition to the amido digermyne **1Ge** into the most important MOs of the fragments. The mixing coefficients that are given in parentheses show that the donor orbital  $\Psi_2$  is mainly composed of the HOMO of **1Ge** and the acceptor orbital  $\Psi_{-2}$  is mainly composed of the LUMO of  $H_2$ . The contributions of further three MOs of the fragments are much smaller.

LUMO of  $H_2$  have the largest absolute coefficients (0.470 and 0.383) in the description of  $\Psi_2$  and  $\Psi_{-2}$ . There are small polarizing contributions of three other orbitals which have coefficients between 0.022 and 0.086).

The EDA–NOCV results of the transition states demonstrate the enormous insight into the interatomic interactions, which is provided by the charge-and energy decomposition method. It serves as a bridge between the descriptive bonding models of chemistry and the explanation of chemical interactions that comes from accurate quantum chemical calculations.

## Conclusion and Perspective

The review demonstrates that the EDA is a very powerful method for a qualitative and quantitative analysis of the chemical bond. The EDA results provide a bridge between the heuristic bonding models which have been developed in synthetic chemistry and the numerical results of accurate quantum chemical calculations. Questions which address for example the multiplicity of chemical bonds or the covalent nature of interatomic interactions can be answered in an

unambiguous way. The trends of bond strengths can be explained in terms of the physically meaningful parameters electrostatic attraction, Pauli repulsion and orbital (covalent) interaction. A strong point of the EDA is the fact that it analyzes the instantaneous interatomic interactions of a chemical bond without referring to an external reference system. The EDA thus provides a coherent picture of the nature of the chemical bonds in terms of chemically useful expressions. The extension to the EDA–NOCV method provides a bridge between MO correlations diagrams and pairwise orbital interactions, which have been shown in the past to correlate with the structures and reactivities of molecules. There is a link between frontier orbital theory and orbital symmetry rules and the quantitative charge- and energy partitioning scheme that is provided by the EDA–NOCV terms. The strength of the pairwise orbital interactions can quantitatively be estimated and the associated change in the electronic structure can be visualized by plotting the deformation densities. The EDA–NOCV method may be used in the future as a quantitative criterion for comparing different types of chemical bonds across the periodic system.

## ACKNOWLEDGEMENT

This work was supported by the Deutsche Forschungsgemeinschaft and by the Alexander von Humboldt Foundation. LZ and GF gratefully acknowledge financial support from Nanjing Tech University (grant numbers 39837132 and 39837123), a SICAM Fellowship from Jiangsu National Synergetic Innovation Center for Advanced Materials, the National Science Foundation of Jiang Su (Grant No. BK20170964), and the National Science Foundation of China (Grant No. 21703099).

## REFERENCES

1. Heitler W, London F. Wechselwirkung neutraler Atome und homöopolare Bindung nach der Quantenmechanik. *Zeitschrift für Physik* 1927; 44:455–472.
2. Several essays and opinions on the role of chemical models in chemical science have been published recently, e.g. WHE S. Chemical bonding: state of the art in conceptual quantum chemistry. An introduction. *Theor Chem Acc* 2001; 105:271–275.
3. Shaik S. Is my chemical universe localized or delocalized? Is there a future for chemical concepts? *New J Chem* 2007; 31:2105–2028.
4. Frenking G, Krapp A. Unicorns in the world of chemical bonding models. *J Comput Chem* 2007; 28:15–24.
5. Lewis GN. The atom and the molecule. *J Am Chem Soc* 1916; 38:762–785.
6. A discussion of the impact and importance of the work of G. N. Lewis to the theory of chemistry is presented in a special issue edited by Frenking G, Shaik S. 90 years of chemical bonding. *J Comput Chem* 2007; 28:1–3.
7. Pauling L. *The nature of the chemical bond and the structure of molecules and crystals*. 3rd ed. Ithaca, NY: Cornell University Press; 1960.
8. Morokuma K. Molecular orbital studies of hydrogen bonds. *J Chem Phys* 1971; 55:1236–1244.
9. Ziegler T, Rauk A. On the calculation of bonding energies by the Hartree Fock Slater method. *Theor Chim Acta* 1977; 46:1–10.
10. Bader RFW. *Atoms in Molecules. A Quantum Theory*. Oxford, UK: Oxford University Press; 1990.
11. Frenking G, von Hopffgarten M. Calculation of bonding properties. In: Solomon EI, Scott RA, King RB, eds. *Computational Inorganic and*

- Bioinorganic Chemistry*. New York: John Wiley & Sons; 2009, 3–16.
- 12. Mitoraj M, Michalak A. Natural orbitals for chemical valence as descriptors of chemical bonding in transition metal complexes. *J Mol Model* 2007, 13:347–355.
  - 13. Mitoraj MP, Michalak A, Ziegler T. A combined charge and energy decomposition scheme for bond analysis. *J Chem Theory Comput* 2009, 5:962–975.
  - 14. Fukui K. *Theory of Orientation and Stereoselection*. Berlin: Springer Verlag; 1975.
  - 15. Woodward RB, Hoffmann R. *The Conservation of Orbital Symmetry*. Verlag Chemie: Weinheim; 1970.
  - 16. Mo YR, Peyerimhoff SD. Theoretical analysis of electronic delocalization. *J Chem Phys* 1998, 109:1687–1697.
  - 17. Mo YR, Gao JL, Peyerimhoff SD. Energy decomposition analysis of intermolecular interactions using a block-localized wave function approach. *J Chem Phys* 2000, 112:5530–5538.
  - 18. Mo YR. Geometrical optimization for strictly localized structures. *J Chem Phys* 2003, 119:1300–1306.
  - 19. Mo YR. Intramolecular electron transfer: computational study based on the orbital deletion procedure (ODP). *Curr Org Chem* 2006, 10:779–790.
  - 20. Mo Y. The block-localized wavefunction (BLW) perspective of chemical bonding. In: Frenking G, Shaik S, eds. *The Chemical Bond 1. Fundamental Aspects of Chemical Bonding*. Weinheim: Wiley-VCH; 2014, 199–232.
  - 21. Cardozo TM, Chaer Nascimento MA. Energy partitioning for generalized product functions: The interference contribution to the energy of generalized valence bond and spin coupled wave functions. *J Chem Phys* 2009, 130:104102.
  - 22. Cardozo TM, Nascimento MAC. Chemical bonding in the N<sub>2</sub> molecule and the role of the quantum mechanical interference effect. *Journal of Physical Chemistry A* 2009, 113:12541–12548.
  - 23. de Sousa DWO, Nascimento MACI. There a quadruple bond in C<sub>2</sub>? *J Chem Theory Comput* 2016, 12:2234–2241.
  - 24. Mo Y, Song L, Lin Y. Block-localized wavefunction (BLW) method at the density functional theory (DFT) level. *J Phys Chem A* 2007, 111:8291–8301.
  - 25. Blanco MA, Martín Pendás A, Francisco E. Interacting quantum atoms: a correlated energy decomposition scheme based on the quantum theory of atoms in molecules. *J Chem Theory Comput* 2005, 1:1096–1109.
  - 26. Pendás AM, Blanco MA, Francisco E. Chemical fragments in real space: definitions, properties, and energetic decompositions. *J Comput Chem* 2007, 28:161–184.
  - 27. Pendás AM, Blanco MA, Francisco E. Steric repulsions, rotation barriers, and stereoelectronic effects: a real space perspective. *J Comput Chem* 2009, 30:98–109.
  - 28. García-Revilla M, Francisco E, Popelier PLA, Martín Pendás A. Domain-averaged exchange-correlation energies as a physical underpinning for chemical graphs. *ChemPhysChem* 2013, 14:1211–1218.
  - 29. Maxwell P, Martin Pendás A, Popelier PLA. Extension of the interacting quantum atoms (IQA) approach to B3LYP level density functional theory (DFT). *Phys Chem Chem Phys* 2016, 18:20986–21000.
  - 30. Khaliullin RZ, Head-Gordon M, Bell AT. An efficient self-consistent field method for large systems of weakly interacting components. *J Chem Phys* 2006, 124:204105-1–204105-11.
  - 31. Khaliullin RZ, Cobar EA, Lochan RC, Bell AT, Head-Gordon M. Unravelling the origin of intermolecular interactions using absolutely localized molecular orbitals. *J Phys Chem A* 2007, 111:8753–8765.
  - 32. Horn PR, Mao Y, Head-Gordon M. Probing non-covalent interactions with a second generation energy decomposition analysis using absolutely localized molecular orbitals. *Phys Chem Chem Phys* 2016, 18:23067–23079.
  - 33. Thirman J, Head-Gordon M. Efficient implementation of energy decomposition analysis for second-order Møller-Plesset perturbation theory and application to anion-π interactions. *Chem A Eur J* 2017, 121:717–728.
  - 34. Horn PR, Sundstrom EJ, Baker TA, Head-Gordon M. Unrestricted absolutely localized molecular orbitals for energy decomposition analysis: theory and applications to intermolecular interactions involving radicals. *J Chem Phys* 2013, 138:134119.
  - 35. Horn PR, Head-Gordon M. Polarization contributions to intermolecular interactions revisited with fragment electric-field response functions. *J Chem Phys* 2015, 143:114111.
  - 36. Levine DS, Horn PR, Mao Y, Head-Gordon M. Variational energy decomposition analysis of chemical bonding. 1. Spin-pure analysis of single bonds. *J Chem Theory Comput* 2016, 12:4812–4820.
  - 37. Azar RJ, Horn PR, Sundstrom EJ, Head-Gordon M. Useful lower limits to polarization contributions to intermolecular interactions using a minimal basis of localized orthogonal orbitals: theory and analysis of the water dimer. *J Chem Phys* 2013, 138:084102.
  - 38. Bitter T, Ruedenberg K, Schwarz WHE. Toward a physical understanding of electron-sharing two-center bonds. I. General aspects. *J Comput Chem* 2007, 28:411–422.
  - 39. Bitter T, Wang SG, Ruedenberg K, Schwarz WHE. Toward a physical understanding of electron-sharing two-center bonds. II. Pseudo-potential based analysis

- of diatomic molecules. *Theor Chem Acc* 2010, 127:237–257.
40. Schmidt MW, Ivanic J, Ruedenberg K. The physical origin of the chemical bond. In: Frenking G, Shaik S, eds. *The Chemical Bond. 1. Fundamental Aspects of Chemical Bonding*. Weinheim: Wiley-VCH; 2014, 1–67.
41. Bickelhaupt FM, Baerends EJ. Kohn Sham density functional theory: predicting and understanding chemistry. In: Lipkowitz KB, Boyd BD, eds. *Reviews in Computational Chemistry*, vol. 15. New York: Wiley-VCH; 2000, 1–86.
42. Wagner JP, Schreiner PR. London dispersion in molecular chemistry—reconsidering steric effects. *Angew Chem Int Ed* 2015, 54:12274–12296.
43. Grimme S. Accurate description of van der Waals complexes by density functional theory including empirical corrections. *J Comput Chem* 2004, 25:1463–1473.
44. Grimme S. Semiempirical GGA-type density functional constructed with a long-range dispersion correction. *J Comput Chem* 2006, 27:1787–1799.
45. Esterhuyzen C, Frenking G. The nature of the chemical bond revisited: An energy decomposition analysis of diatomic molecules  $E_2$  ( $E=N\text{-Bi}$ ,  $F\text{-I}$ ), CO and BF. *Theor Chem Acc* 2004, 111:381–389.
46. Kovács A, Esterhuyzen C, Frenking G. The nature of the chemical bond revisited: an energy partitioning analysis of nonpolar bonds. *Chem – A Eur J* 2005, 11:1813–1823.
47. Krapp A, Bickelhaupt FM, Frenking G. Orbital overlap and chemical bonding. *Chem – A Eur J* 2006, 12:9196–9216.
48. Spackman MA, Maslen EN. Chemical properties from the promolecule. *J Phys Chem* 1986, 90:2020–2027.
49. Loschen C, Voigt K, Frunzke J, Diefenbach A, Diedenhofen M, Frenking G. Quantum chemical investigations of the phosphane complexes  $X_3\text{B-PY}_3$  and  $X_3\text{Al-PY}_3$  ( $X = \text{H, F, Cl}$ ;  $Y = \text{F, Cl, Me, CN}$ ). *Zeitschrift für anorganische und allgemeine Chemie* 2002, 628:1294–1304.
50. Bessac F, Frenking G. Chemical bonding in phosphane and amine complexes of main group elements and transition metals. *Inorg Chem* 2003, 42:7990–7994.
51. Frenking G, Wichmann K, Fröhlich N, Loschen C, Lein M, Frunzke J, Rayón VM. Towards a rigorously defined quantum chemical analysis of the chemical bond in donor-acceptor complexes. *Coord Chem Rev* 2003, 238–239:55–82.
52. Cappel D, Tüllmann S, Krapp A, Frenking G. Direct estimate of the conjugative and hyperconjugative stabilization in diynes, dienes and related compounds. *Angew Chem Int Ed* 2005, 44:3617–3620 *Angew Chem* 117:3683–3686.
53. Fernández I, Frenking G. Direct estimate of the strength of conjugation and hyperconjugation by the energy decomposition analysis method. *Chem A Eur J* 2006, 12:3617–3629.
54. Fernández I, Frenking G. Direct estimate of conjugation and aromaticity in cyclic compounds with the EDA method. *Faraday Discuss* 2007, 135:403–421.
55. Hückel E. Quantentheoretische Beiträge zum Benzolproblem. I. Die Elektronenkonfiguration des Benzols und verwandter Verbindungen. *Zeitschrift für Physik* 1931, 70:204–286.
56. Hückel E. Quantentheoretische Beiträge zum Benzolproblem. II. Quantentheorie der induzierten Polaritäten. *Zeitschrift für Physik* 1931, 72:310–337.
57. Hückel E. Quantentheoretische Beiträge zum Problem der aromatischen und ungesättigten Verbindungen. III. *Zeitschrift für Physik* 1932, 76:628–648.
58. Hückel E. Die freien Radikale der organischen Chemie. Quantentheoretische Beiträge zum Problem der aromatischen und ungesättigten Verbindungen. IV. *Zeitschrift für Physik* 1933, 83:632–668.
59. Doering W v E, Detert FL. Cycloheptatrienylium oxide. *J Am Chem Soc* 1951, 73:876–877.
60. von Ragué Schleyer P. The theoretical treatment of aromaticity is topic of a special issue entitled “Aromaticity”. *Chem Rev* 2001, 101:1115–1118.
61. von Ragué Schleyer P. for reviews on conjugation and delocalization see the special issue entitled “Delocalization – pi and sigma”. *Chem Rev* 2005, 105:3433–3435.
62. See Refs 60, 61 A detailed review on different ways to estimate aromaticity is given in: Mo Y, von Ragué Schleyer P. An energetic measure of aromaticity and antiaromaticity based on the Pauling-Wheland resonance energies. *Chem A Eur J* 2006, 12:2009–2020.
63. Thorn DL, Hoffmann R. Delocalization in metallocycles. *Nouveau J de Chimie* 1979, 3:39–45.
64. Fernández I, Frenking G. Aromaticity in Metallabenzenes. *Chem A Eur J* 2007, 13:5873–5884.
65. Pierrefixe SCAH, Bickelhaupt FM. Aromaticity: molecular-orbital picture of an intuitive concept. *Chem A Eur J* 2007, 13:6321–6328.
66. Pierrefixe SCAH, Bickelhaupt FM. Aromaticity and antiaromaticity In 4-, 6-, 8-, and 10-membered conjugated hydrocarbon rings. *J Phys Chem A* 2008, 12:12816–12822.
67. Shaik SS, Hiberty PC. When does electronic delocalization become a driving force of molecular shape and stability? 1. The aromatic sextet. *J Am Chem Soc* 1985, 107:3089–3095.
68. Diefenbach A, Bickelhaupt FM, Frenking G. The nature of the transition metal-carbonyl bond and the question about valence orbitals of transition metals. a bond-energy decomposition analyses of  $\text{TM}(\text{CO})_6^q$

- (TM<sup>q</sup> = Hf<sup>2+</sup>, Ta<sup>-</sup>, W, Re<sup>+</sup>, Os<sup>2+</sup>, Ir<sup>3+</sup>). *J Am Chem Soc* 2000, 122:6449–6458.
69. Nechaev MS, Rayón VM, Frenking GF. Energy partitioning analysis of the bonding in ethylene and acetylene complexes of group 6, 8, and 11 metals: (CO)<sub>5</sub>TM-C<sub>2</sub>H<sub>x</sub> and Cl<sub>4</sub>TM-C<sub>2</sub>H<sub>x</sub> (TM=Cr, Mo, W), (CO)<sub>4</sub>TM-C<sub>2</sub>H<sub>x</sub> (TM = Fe, Ru, Os), and TM<sup>+</sup>-C<sub>2</sub>H<sub>x</sub> (TM=Cu, Ag, Au). *J Phys Chem A* 2004, 108:3134–3142.
  70. Tonner R, Heydenrych G, Frenking G. Bonding analysis of N-heterocyclic carbene tautomers and phosphine ligands in transition metal complexes: a theoretical study. *Chem Asian J* 2007, 2:1555–1567.
  71. Frenking G, Wichmann K, Fröhlich N, Grobe J, Golla W, Van DL, Krebs B, Läge M. Nature of the metal-ligand bond in M(CO)<sub>3</sub>PX<sub>3</sub> complexes (M = Cr, Mo, W; X = H, Me, F, Cl): synthesis, molecular structure, and quantum-chemical calculations. *Organometallics* 2002, 21:2921–2930.
  72. Dewar MJS. A review of the  $\pi$ -complex-theory. *Bull Soc Chim France* 1951, 18C:74–79.
  73. Chatt J, Duncanson LA. Olefin co-ordination compounds. Part III. Infra-red spectra and structure: attempted preparation of acetylene complexes. *J Chem Soc* 1953:2939–2947.
  74. Frenking G. Understanding the nature of the bonding in transition metal complexes: from dewar's molecular orbital model to an energy partitioning analysis of the metal-ligand bond. *J Organomet Chem* 2001, 635:9–23.
  75. Frenking G. The Dewar-Chatt-Duncanson bonding model of transition metal-olefin complexes examined by modern quantum chemical methods. In: Leigh GJ, Winterton N, eds. *Modern Coordination Chemistry: The Legacy of Joseph Chatt*. London: The Royal Society; 2002, 111.
  76. Heydenrych G, von Hopffgarten M, Stander E, Schuster O, Raubenheimer HG, Frenking G. The nature of the metal-carbene bond in normal and abnormal pyridylidene, quinolylidene and isoquinolylidene complexes. *Eur J Inorg Chem* 2009, 2009:1892–1904.
  77. Nemcsok D, Wichmann K, Frenking G. The significance of  $\pi$  interactions in group 11 complexes with N-heterocyclic carbenes. *Organometallics* 2004, 23:3640–3646.
  78. Rayón VM, Frenking G. Bis(benzene)chromium is a  $\delta$ -bonded molecule and ferrocene is a  $\pi$ -bonded molecule. *Organometallics* 2003, 22:3304–3308.
  79. Miller SA, Tebboth JA, Tremaine JF. Dicyclopentadienyliron. *J Chem Soc* 1952:632–635.
  80. Kealy TJ, Pauson PL. A new type of organo-iron compound. *Nature* 1951, 168:1039–1040.
  81. Fischer EO, Pfab W, Zur Kristallstruktur D. Di-cyclopentadienyl-verbindungen des zweiwertigen eisens, kobalts und nickels. *Zeitschrift für Naturforschung* 1952, 7B:377–379.
  82. Wilkinson G, Rosenblum M, Whiting MC, Woodward RB. The structure of iron bis-cyclopentadienyl. *J Am Chem Soc* 1952, 74:2125–2126.
  83. Elschenbroich C, ed. *Organometallics*. 3rd ed. Weinheim: Wiley-VCH; 2006.
  84. Fischer EO, Hafner W. Di-benzol-chrom. *Zeitschrift für Naturforschung* 1955, 10B:665–668.
  85. A historical review of the way to the synthesis of chromium bisbenzene and the subsequent development of organometallic chemistry is illustrated in two reviews: Seyerth D. Bis(benzene)chromium. 1. Franz Hein at the University of Leipzig and Harold Zeiss and Minoru Tsutsui at Yale. *Organometallics* 2002, 21:1520–1530.
  86. Seyerth D. Bis(benzene)chromium. 2. Its Discovery by E. O. Fischer and W. Hafner and Subsequent Work by the Research Groups of E. O. Fischer, H.-H. Zeiss, F. Hein, C. Elschenbroich, and Others. *Organometallics* 2002, 21:2800–2820.
  87. Cadenbach T, Bollermann T, Gemel C, Fernández I, von Hopffgarten M, Frenking G, Fischer RA. Twelve one-electron ligands coordinating one metal center: structure and bonding of [Mo(ZnCH<sub>3</sub>)<sub>9</sub>(ZnCp<sup>\*</sup>)<sub>3</sub>]. *Angew Chem Int Ed* 2008, 47:9150–9154 *Angew Chemie* 2008, 120:9290–9295.
  88. Lein M, Frunzke J, Timoshkin A, Frenking G. Iron bispentazole Fe( $\eta^5$ -N<sub>5</sub>)<sub>2</sub>, a theoretically predicted high-energy compound: structure, bonding analysis, metal-ligand bond strength and a comparison with the isoelectronic ferrocene. *Chem A Eur J* 2001, 7:4155–4163.
  89. Frunzke J, Lein M, Frenking G. Structures, metal-ligand bond strength, and bonding analysis of ferrocene derivatives with group-15 heteroligands Fe( $\eta^5$ -E<sub>5</sub>)<sub>2</sub> and FeCp( $\eta^5$ -E<sub>5</sub>) (E = N, P, As, Sb). A theoretical study. *Organometallics* 2002, 21:3351–3359.
  90. Lein M, Frunzke J, Frenking G. Structures and bonding of the sandwich complexes [Ti( $\eta^5$ -E<sub>5</sub>)<sub>2</sub>]<sup>2-</sup> (E = CH, N, P, As, Sb): a theoretical study. *Inorg Chem* 2003, 42:2504–2511.
  91. Rayón VM, Frenking G. Structures, bond energies, heats of formation, and quantitative bonding analysis of main group metallocenes [E(Cp)<sub>2</sub>] (E = Be-Ba, Zn, Si-Pb) and [E(Cp)] (E = Li-Cs, B-Tl). *Chem A Eur J* 2002, 8:4693–4707.
  92. Resa I, Carmona E, Gutierrez-Puebla E, Monge A. Decamethyldizincocene, a stable compound of Zn(I) with a Zn-Zn bond. *Science* 2004, 305:1136–1138.
  93. Velazquez A, Fernández I, Frenking G, Merino G. Multimetallocenes. A theoretical study. *Organometallics* 2007, 26:4731–4736.

94. Esenturk EN, Fettinger J, Lam Y-F, Eichhorn B.  $[Pt@Pb_{12}]^{2-}$ . *Angew Chem Int Ed* 2004, 43:2132–2134 *Angew Chem* 116:2184–2186.
95. Esenturk EN, Fettinger J, Eichhorn B. The  $Pb_{12}^{2-}$  and  $Pb_{10}^{2-}$  zintl ions and the  $M@Pb_{12}^{2-}$  and  $M@Pb_{10}^{2-}$  cluster series where M=Ni, Pd, Pt. *J Am Chem Soc* 2006, 128:9178–9186.
96. Wade K. Structural and bonding patterns in cluster chemistry. *Adv Inorg Chem Radiochem* 1976, 18:1–66.
97. Mingos DMP. Polyhedral skeletal electron pair approach. *Acc Chem Res* 1984, 17:311–319.
98. Chen M, Zhang Q, Zhou M, Andrade DM, Frenking G. Carbon monoxide bonding with BeO and  $BeCO_3$ : surprisingly high CO stretching frequency of  $OCBeCO_3$ . *Angew Chem Int Ed* 2015, 54:124–128.
99. Zhan C-G, Liu F, Hu Z-M. Bond strength and bond angles for hybrid orbitals composed of arbitrary sets of orbital angular momentum quantum number. *Int J Quant Chem* 1987, 32:13–18.
100. Firman TK, Landis CR. Structure and electron counting in ternary transition metal hydrides. *J Am Chem Soc* 1998, 120:12650–12656.
101. Fukui K. The path of chemical reactions—The IRC approach. *Acc Chem Res* 1981, 14:363–372.
102. Bickelhaupt FM, Baerends EJ, Nibbering NMM, Ziegler T. Theoretical investigation on base-induced 1,2-eliminations in the model system  $F^- + CH_3CH_2F$ . The role of the base as a catalyst. *J Am Chem Soc* 1993, 115:9160–9173.
103. Fernández I, Frenking G, Uggerud E. The interplay of steric and electronic effects in  $S_N2$  reactions. *Chem A Eur J* 2009, 15:2166–2175.
104. Bento AP, Bickelhaupt FM. Nucleophilicity and leaving-group ability in frontside and backside  $S_N2$  reactions. *J Org Chem* 2008, 73:7290–7299.
105. de Jong GT, Bickelhaupt FM. Transition state energy and position along the reaction coordinate in an extended activation strain model. *ChemPhysChem* 2007, 8:1170–1181.
106. van Zeist W-J, Visser R, Bickelhaupt FM. The steric nature of the bite angle. *Chem A Eur J* 2009, 15:6112–6115.
107. Bickelhaupt FM, Ziegler T, von Ragué Schleyer P. Oxidative insertion as frontside  $S_N2$  substitution: a theoretical study of the model reaction system Pd +  $CH_3Cl$ . *Organometallics* 1995, 14:2288–2296.
108. Diefenbach A, Bickelhaupt FM. Oxidative addition of Pd to C-H, C-C and C-Cl bonds: importance of relativistic effects in DFT calculations. *J Chem Phys* 2001, 115:4030–4040.
109. Diefenbach A, Bickelhaupt FM. Activation of H-H, C-H, C-C, and C-Cl bonds by Pd(0). Insight from the activation strain model. *J Phys Chem A* 2004, 108:8460–8466.
110. Diefenbach A, de Jong GT, Bickelhaupt FM. Activation of H-H, C-H, C-C and C-Cl bonds by Pd and  $PdCl^-$ . understanding anion assistance in C-X bond activation. *J Chem Theory Comput* 2005, 1:286–298.
111. Diefenbach A, Bickelhaupt FM. Activation of C-H, C-C and C-I bonds by Pd and *cis*- $Pd(CO)_2I_2$ . Catalyst-substrate adaption. *J Organomet Chem* 2005, 690:2191–2199.
112. de Jong GT, Bickelhaupt FM. Catalytic carbon-halogen activation: trends in reactivity, selectivity, and solvation. *J Chem Theory Comput* 2007, 3:514–529.
113. de Jong GT, Visser R, Bickelhaupt FM. Oxidative addition to main group versus transition metals: insight from the activation strain model. *J Organomet Chem* 2006, 691:4341–4349.
114. van Stralen JNP, Bickelhaupt FM. Oxidative addition versus dehydrogenation of methane, silane, and heavier  $AH_4$  congeners reacting with palladium. *Organometallics* 2006, 25:4260–4268.
115. Fernández I, Bickelhaupt FM, Cossío FP. Double group transfer reactions: role of activation strain and aromaticity in reaction barriers. *Chem A Eur J* 2009, 15:13022–13032.
116. Bickelhaupt FM. Understanding reactivity with Kohn-Sham molecular orbital theory:  $E2-S_N2$  mechanistic spectrum and other concepts. *J Comput Chem* 1999, 20:114–128.
117. van Zeist W-J, Bickelhaupt FM. The activation strain model of chemical reactivity. *Org Biomol Chem* 2010, 8:3118–3127.
118. Fernandez I, Bickelhaupt FM. Deeper insight into the Diels-Alder reaction through the activation strain model. *Chem Asian J* 2016, 11:3297–3304.
119. Lein M, Krapp A, Frenking G. Why do the heavy-atom analogues of acetylene  $E_2H_2$  ( $E = Si - Pb$ ) exhibit unusual structures? *J Am Chem Soc* 2005, 127:6290–6299.
120. Pu L, Twamley B, Power PP. Synthesis and characterization of  $2,6-Trip_2H_3C_6PbPbC_6H_3-2,6-Trip_2$  ( $Trip = C_6H_2-2,4,6-i-Pr_3$ ): a stable heavier group 14 element analogue of an alkyne. *J Am Chem Soc* 2000, 122:3524–3525.
121. Phillips AD, Wright RJ, Olmstead MM, Power PP. Synthesis and characterization of  $2,6-Dipp_2H_3C_6SnSnC_6H_3-2,6-Dipp_2$  ( $Dipp = C_6H_3-2,6-Pr^i_2$ ): a tin analogue of an alkyne. *J Am Chem Soc* 2002, 124:5930–5931.
122. Stender M, Phillips AD, Wright RJ, Power PP. Synthesis and characterization of a digermanium analogue of an alkyne. *Angew Chem Int Ed* 2002, 41:1785–1787 *Angew Chem* 2002, 114:1863–1865.

123. Sekiguchi A, Kinjo R, Ichinohe MA. Stable compound containing a silicon-silicon triple bond. *Science* 2007, 305:1755–1757.
124. Jacobsen H, Ziegler T. Nonclassical double bonds in ethylene analogues: influence of pauli repulsion on trans bending and  $\pi$  bond strength. A density functional study. *J Am Chem Soc* 1994, 116:3667–3679.
125. Ziegler T. Theoretical study of the triple metal bond in  $d^3-d^3$  binuclear complexes of chromium, molybdenum, and tungsten by the Hartree-Fock-Slater transition state method. *J Am Chem Soc* 1983, 105:7543–7549.
126. Ziegler T. Theoretical study of multiple metal-metal bonds in binuclear complexes of group 6D and group 7D transition elements with the general formula  $M_2Cl_4(PH_3)_4^{n+}$  ( $n = 0, 1, 2$ ) by the Hartree-Fock-Slater transition state method. *J Am Chem Soc* 1984, 106:5901–5908.
127. Krapp A, Lein M, Frenking G. The strength of the  $\sigma$ -,  $\pi$ - and  $\delta$ -bonds in  ${}^2\text{Re}_2\text{Cl}_8$ . *Theor Chem Acc* 2008, 120:313–320.
128. Koch W, Collins JR, Frenking G. Are there neutral helium compounds which are stable in their ground state? A theoretical investigation of HeBCH and HeBeO. *Chem Phys Lett* 1986, 132:330–333.
129. Koch W, Frenking G, Gauss J, Cremer D, Collins JB. Helium chemistry: theoretical predictions and experimental challenge. *J Am Chem Soc* 1987, 109:5917–5931.
130. Frenking G, Koch W, Gauss J, Cremer D. Stabilities and nature of the attractive interactions in HeBeO, NeBeO, ArBeO and a comparison with analogues NGLiF, NGBN and NGLiH (NG = He, Ar). A theoretical investigation. *J Am Chem Soc* 1988, 110:8007–8016.
131. Andrews L, Tague TJ. Reactions of pulsed-laser evaporated be atoms with  $\text{CO}_2$ -infrared spectra of OCBeO and COBeO in solid argon. *J Am Chem Soc* 1994, 116:6856–6859.
132. Frenking G, Koch W, Collins JR. Fixation of nitrogen and carbon monoxide by beryllium oxide: theoretical investigation of the structures and stabilities of NNBeO, OCBeO and COBeO. *J Chem Soc Chem Commun* 1988:1147–1148.
133. When CO is bonded via a  $\sigma$ -bond to a Lewis acid A at the carbon end A $\leftarrow$ CO the bond becomes shorter and stronger, but  $\sigma$ -bonding at oxygen A $\leftarrow$ OC weakens the bond. This can be explained with the change in the polarization of the orbitals: Lupinetti AJ, Fau S, Frenking G, Strauss SH. Theoretical analysis of the bonding between CO and positively charged atoms. *J Phys Chem A* 1997, 101:9551–9559.
134. Lupinetti AJ, Frenking G, Strauss SH. Nonclassical metal carbonyls: appropriate definitions with a theoretical justification. *Angew Chem Int Ed* 1998, 37:2113–2116.
135. Lupinetti AJ, Strauss SH, Frenking G. Nonclassical metal carbonyls. *Prog Inorg Chem* 2001, 49:1–112.
136. Diels O, Wolf B. Über das Kohlensuboxyd. *Berichte der Deutschen Chemischen Gesellschaft* 1906, 39:689–697.
137. Zhang Q, Li WL, Xu C, Chen M, Zhou M, Li J, Andrade DM, Frenking G. Formation and characterization of the boron dicarbonyl complex  $[\text{B}(\text{CO})_2]^-$ . *Angew Chem* 2015, 127:11230–11235 *Angew Chem Int Ed* 2015, 54: 11078–11083.
138. Jensen P, Johns JWC. The infrared spectrum of carbon suboxide in the  $\nu_6$  fundamental region: experimental observation and semirigid bender analysis. *J Mol Spectr* 1986, 118:248–266.
139. Koput J. An ab initio study on the equilibrium structure and CCC bending energy levels of carbon suboxide. *Chem Phys Lett* 2000, 320:237–244.
140. Carbon suboxide has a very flat bending potential and becomes linear in the solid state, which is due to intermolecular interactions: Ellern A, Drews T, Seppelt K. The structure of carbon suboxide,  $\text{C}_3\text{O}_2$ , in the solid state. *Zeitung für Anorganische und Allgemeine Chemie* 2001, 627:73–76.
141. Bernhardi I, Drews T, Seppelt K. Isolation and structure of the  $\text{OCNCO}^+$  ion. *Angew Chem* 1999, 111:2370–2372 *Angew Chem Int Ed* 1999, 38: 2232–2233.
142. Zhang Q, Li WL, Xu C, Chen M, Zhou M, Li J, Andrade DM, Frenking G. Formation and characterization of the boron dicarbonyl complex  $[\text{B}(\text{CO})_2]^-$ . *Angew Chem* 2015, 127:11230–11235 *Angew Chem Int Ed* 2015, 54: 11078–11083.
143. Celik MA, Frenking G, Neumüller B, Petz W. Exploiting the twofold donor ability of carbodiphosphoranes. Theoretical studies of  $[(\text{PPh}_3)_2\text{C}\rightarrow\text{EH}_2]^q$  ( $\text{E}^q = \text{Be}, \text{B}^+, \text{C}^{2+}, \text{N}^{3+}, \text{O}^{4+}$ ) and synthesis of the dication  $[(\text{Ph}_3\text{P})_2\text{C}=\text{CH}_2]^{2+}$ . *ChemPlusChem* 2013, 78:1024–1032.
144. Andrade DM, Frenking G. Stabilization of heterodiatomic SiC through ligand donation. Theoretical investigation of  $\text{SiC}(\text{L})_2$  ( $\text{L} = \text{NHC}^{\text{Me}}, \text{CAAC}^{\text{Me}}, \text{PMes}_3$ ). *Angew Chem Int Ed* 2015, 54:12319–12324 *Angew Chem* 2015, 127: 12494–12500.
145. Mohapatra C, Kundu S, Paesch AN, Herbst-Irmer R, Stalke D, Andrade DM, Frenking G, Roesky HW. The structure of the carbene stabilized  $\text{Si}_2\text{H}_2$  may be equally well described with coordinate bonds as with classical double bond. *J Am Chem Soc* 2016, 138:10429–10432.
146. Georgiou DC, Zhao L, Wilson DJD, Frenking G, Dutton JL. NHC stabilized acetylene – how far can the analogy be pushed? *Chem A Eur J* 2017, 23:2926–2934.

147. Li Z, Chen X, Andrade DM, Frenking G, Benkő Z, Li Y, Harmer J, Su CY, Grützmacher H. ( $L_2C_2P_2$ , dicarbodiphosphide stabilized by N-heterocyclic carbenes or cyclic diamido carbenes. *Angew Chem* 2017, 129:5838–5843 *Angew Chem Int Ed* 2017, 56: 5744–5749.
148. Tonner R, Öxler F, Neumüller B, Petz W, Frenking G. Carbodiphosphoranes: the chemistry of divalent carbon(0). *Angew Chem* 2006, 118:8206–8211 *Angew Chem Int Ed* 2006, 45: 8038–8042.
149. For reviews see: Frenking G, Tonner R, Klein S, Takagi N, Shimizu T, Krapp A, Pandey KK, Parameswaran P. New bonding modes of carbon and heavier group 14 atoms Si – Pb. *Chem Soc Rev* 2014, 43:5106–5139.
150. Zhao L, Hermann M, Holzmann N, Frenking G. Dative bonding in main group compounds. *Coord Chem Rev* 2017, 344:163–204. <https://doi.org/10.1016/j.ccr.2017.03.026>.
151. Frenking G, Tonner R. Divalent carbon(0) compounds. *Pure Appl Chem* 2009, 81:597–614.
152. Ramirez F, Desai NB, Hansen B, McKelvie N. Hexaphenylcarbodiphosphorane ( $C_6H_5)_3PCP(C_6H_5)_3$ . *J Am Chem Soc* 1961, 83:3539–3540.
153. Tonner R, Frenking G. Divalent carbon(0) chemistry, part 1: parent compounds. *Chem A Eur J* 2008, 14:3260–3272.
154. Tonner R, Frenking G. Divalent carbon(0) chemistry, part 2: protonation and complexes with main group and transition metal lewis acids. *Chem A Eur J* 2008, 14:3273–3289.
155. Tonner R, Frenking G.  $C(NHC)_2$ : divalent carbon (0) compounds with N-heterocyclic carbene ligands – theoretical evidence for a class of molecules with promising chemical properties. *Angew Chem* 2007, 119:8850–8853 *Angew Chem Int Ed* 2007, 46: 8695–8698.
156. For a detailed description of carbodicarbenes see: Frenking G, Tonner R. Carbodicarbenes — divalent carbon(0) compounds exhibiting carbon–carbon donor–acceptor bonds. *Wiley Interdiscip Rev Comput Mol Sci* 2011, 1:869–878.
157. Herrmann WA. N-Heterocyclic carbenes: a new concept in organometallic catalysis. *Angew Chem* 2002, 114:1342–1351 *Angew Chem Int Ed* 2002, 41: 1290–1309.
158. Dyker CA, Lavallo V, Donnadieu B, Bertrand G. Synthesis of an extremely bent acyclic allene (a “carbodicarbene”): a strong donor ligand. *Angew Chem Int Ed* 2008, 47:3206–3209.
159. Alcarazo M, Lehmann W, Anoop A, Thiel W, Fürstner A. Coordination chemistry at carbon. *Nat Chem* 2009, 1:295–301.
160. Fürstner A, Alcarazo M, Goddard R, Lehmann CW. Coordination chemistry of ene-1, 1-diamines and a prototype carbodicarbene. *Angew Chem* 2008, 120:3254–3258 *Angew Chem Int Ed* 2008, 47: 3210–3214.
161. Andrade DM, Holzmann N, Frenking G. Bonding analysis of ylidone complexes  $EL_2$  ( $E = C - Pb$ ) with phosphine and carbene ligands L. *Can J Chem* 2016, 94:1006–1014.
162. Holzmann N, Stasch A, Jones C, Frenking G. Structures and stabilities of group 13 adducts  $[(NHC)(EX_3)]$  and  $[(NHC)_2(E_2X_n)]$  ( $E = B$  to In;  $X = H, Cl$ ;  $n = 4, 2, 0$ ; NHC = N-heterocyclic carbene) and the search for hydrogen storage systems: a theoretical study. *Chem A Eur J* 2011, 17:13517–13525.
163. Pyykö P, Atsumi M. Molecular double-bond covalent radii for elements Li–E112. *Chem A Eur J* 2009, 15:12770–12779.
164. Braunschweig H, Dewhurst RD, Hammond K, Mies J, Radacki K, Vargas A. Ambient-temperature isolation of a compound with aboron-boron triple bond. *Science* 2012, 336:1420–1422.
165. See also: Frenking G, Holzmann N. A boron–boron triple bond. *Science* 2012, 336:1394–1395.
166. Two related complexes with saturated NHC<sup>R</sup> ligands and cAAC (cyclic Alkyl Amino Carbene) groups have in the meantime been isolated: Böhneke J, Braunschweig H, Ewing WC, Hörl C, Kramer T, Krummenacher I, Mies J, Vargas A. Diburabutatriene: an electron-deficient cumulene. *Angew Chem Int Ed* 2014, 53:9082–9085.
167. Böhneke J, Braunschweig H, Dellermann T, Ewing WC, Hammond K, Jimenez-Halla JOC, Kramer T, Mies J. The synthesis of  $B_2(SIDip)_2$  and its reactivity between the diboracumulenic and diborynic extremes. *Angew Chem Int Ed* 2015, 54:13801–13805.
168. Zhou M, Tsumori N, Li Z, Fan K, Andrews L. OCBBCO: A neutral molecule with some boron–boron triple bond character. *J Am Chem Soc* 2002, 124:12936–12937.
169. Papakondylis A, Miliordos E, Mavridis A. Carbonyl boron and related systems: an ab initio study of B–X and YB<sup>+</sup>BY ( $^1\Sigma_g^+$ ), where X = He, Ne, Ar, Kr, CO, CS, N<sub>2</sub> and Y = Ar, Kr, CO, CS, N<sub>2</sub>. *J Phys Chem A* 2004, 108:4335–4340.
170. Ducati LC, Takagi N, Frenking G. Molecules with all triple bonds: OCBBCO, N<sub>2</sub>BBN<sub>2</sub> and [OB<sup>+</sup>BBBO<sup>2-</sup>]. *J Phys Chem A* 2009, 113:11693–11698.
171. Koppe R, Schnöckel H. The boron–boron triple bond? A thermodynamic and force field based interpretation of the N-heterocyclic carbene (NHC) stabilization procedure. *Chem Sci* 2015, 6: 1199–1205.

172. Holzmann N, Hermann M, Frenking G. The boron-boron triple bond in  $\text{NHC}\rightarrow\text{B}\equiv\text{B}\leftarrow\text{NHC}$ . *Chem Sci* 2015, 6:4089–4094. The EDA-NOCV results in this work slightly differ from the data in Table 13, because a different basis set was used.
173. Böhnke J, Braunschweig H, Constantinidis P, Dellermann T, Ewing WC, Fischer I, Hammond K, Hupp F, Mies J, Schmitt HC, Vargas A. Experimental assessment of the strengths of B-B triple bonds. *J Am Chem Soc* 2015, 137:1766–1769.
174. Perras FA, Ewing WC, Dellermann T, Bohnke J, Ullrich S, Schafer T, Braunschweig H, Bryce DL. Spying on the boron-boron triple bond using spin-spin coupling measured from  $^{11}\text{B}$  solid-state NMR spectroscopy. *Chem Sci* 2015, 6:3378–3382.
175. The unpaired electrons in the  $\text{X}^3\Sigma_g^-$  state of  $\text{B}_2$  are in the  $1\pi_u$  and  $1\pi_{u'}$  MOs which are orthogonal to each other (Figure 11). The planes of the two  $\text{NHC}^{\text{Me}}$  ligands in  $\text{B}_2(\text{NHC}^{\text{Me}})_2$  are also nearly perpendicular and therefore they can easily form  $\pi$  MOs. The dihedral angle between the ligand planes deviates from  $90^\circ$  and therefore, the  $\pi$  bonding contributions have different values.
176. Fleming I. *Frontier Orbitals and Organic Chemical Reactions*. New York: John Wiley & Sons; 1976. A new edition has been published with the slightly altered title: *Molecular Orbitals and Organic Chemical Reactions*. New York: John Wiley & Sons; 2010.
177. Hermann M, Goedecke C, Jones C, Frenking G. Reaction pathways for addition of  $\text{H}_2$  to amido-ditetrylynes  $\text{R}_2\text{N}-\text{EE}-\text{NR}_2$  ( $\text{E} = \text{Si}, \text{Ge}, \text{Sn}$ ). A theoretical study. *Organometallics* 2013, 32: 6666–6673.